haematologica
Journal of the Ferrata Storti Foundation

SIRT3 deSUMOylation sustains hematopoietic stem cell activities under stressful conditions via the DHX58-IRF7 axis

by Xiaoxiao He, Jing Yu, Yilu Xu, Tianshi Wang, Yang Lu, Jiaxin Wu, Sijia Dan, Yiqiu Xia, Xingmei Mu, Li Xie, Chiqi Chen, Zhuo Yu, Jing Ye, Eric Gilson, Yaping Zhang, Jinke Cheng and Junke Zheng

Received: October 15, 2025.
Accepted: April 24, 2026.

Citation: Xiaoxiao He, Jing Yu, Yilu Xu, Tianshi Wang, Yang Lu, Jiaxin Wu, Sijia Dan, Yiqiu Xia, Xingmei Mu, Li Xie, Chiqi Chen, Zhuo Yu, Jing Ye, Eric Gilson, Yaping Zhang, Jinke Cheng and Junke Zheng. SIRT3 deSUMOylation sustains hematopoietic stem cell activities via the DHX58-IRF7 axis,
Haematologica. 2026 Apr 30. doi: 10.3324/haematol.2025.300025 [Epub ahead of print]

SIRT3 deSUMOylation sustains hematopoietic stem cell activities under stressful conditions via the DHX58-IRF7 axis

Xiaoxiao He[1,2#*], Jing Yu[1#], Yilu Xu[1#], Tianshi Wang[3,4], Yang Lu[1], Jiaxin Wu[1], Sijia Dan[1], Yiqiu Xia[1], Xingmei Mu[1], Li Xie[1], Chiqi Chen[1], Zhuo Yu[1], Jing Ye[5,6,7], Eric Gilson[5,8,9*], Yaping Zhang[1*], Jinke Cheng[3,10,11*], Junke Zheng[1,12*]

[1] Institute for Translational Medicine on Cell Fate and Disease, Shanghai Ninth People's Hospital, Key Laboratory of Cell Differentiation and Apoptosis of National Ministry of Education, Department of Pathophysiology, Shanghai Jiao Tong University School of Medicine, Shanghai 200025, China.

[2] Department of Hematology, Xinhua Hospital, Shanghai Jiao Tong University School of Medicine, Shanghai 200092, China.

[3] Shanghai Key Laboratory for Tumor Microenvironment and Inflammation, Department of Biochemistry and Molecular Cell Biology, Shanghai Jiao Tong University School of Medicine, Shanghai 200025, China.

[4] Department of Nephrology, Renji Hospital, Shanghai Jiao Tong University School of Medicine, Shanghai 200127, China.

[5] International Laboratory in Hematology, Cancer, Aging and Hematology, Pôle Sino-Français de Recherche en Sciences du Vivant et Génomique, RuiJin Hospital, Shanghai Jiao Tong University School of Medicine/CNRS/INSERM/University Côte d'Azur, Shanghai 200025, China.

[6] The State Key Laboratory of Medical Genomics, Shanghai, 200025, China.

[7] Department of Geriatrics, Medical center on Aging of Shanghai Ruijin Hospital, Shanghai Jiaotong University School of Medicine, Shanghai 200025, China.

[8] University Côte d'Azur, Inserm, CNRS, IRCAN, Nice, France.

[9] Department of medical genetics, IHU RespirERA, CHU, Nice, France.

[10] Institute of Aging & Tissue Regeneration, RenJi Hospital, Shanghai Jiao Tong University School of Medicine, Shanghai 200127, China.

[11] Hainan Academy of Medical Sciences, Haikou Hainan 570102, China.

[12] Shanghai Key Laboratory of Reproductive Medicine, Shanghai Jiao Tong University School of Medicine, Shanghai 200025, China.

[#] These authors contribute equally

***, Corresponding author:** Junke Zheng, 280 South Chongqing Road, Shanghai 200025, China, Email: zhengjunke@shsmu.edu.cn

Authorship Contributions

X.H., J.Y., Y.X., E.G., Y.Z., J.C. and J.Z. designed the experiments, performed the experiments, analyzed data and wrote the paper; T.W., Y.L., J.W., S.D., Y.X., X.M., L.X., C.C., Z.Y., and J.Y. performed the experiments, provided reagents and helped with the manuscript preparation.

Competing interests

The authors declare no competing interests.

Data availability

Statistical analysis was performed using GraphPad software (Prism 10.0). Data are represented as Mean ± SD unless indicated elsewhere. All the experiments were performed independently for at least 3 times. Data were analyzed with a Student's t test

(two-tailed), one-way ANOVA with Tukey's multiple comparison test, or two-way ANOVA with Sidak's multiple comparison test accordingly and statistical significance was set at $P<0.05$ (*P <0.05; **P<0.01; ***P<0.001).

Raw RNA-seq and CUT&Tag-seq data have been deposited in the NCBI Sequence Read Archive (SRA) database (PRJNA1259606, PRJNA1260697).

Acknowledgments

This work was supported by grants from National Basic Research Program of China (2024YFA1803500), National Natural Science Foundation of China (32030030, 82430007, 32100906, 82470121, 82170175, 32371160, 82370180), Postdoctoral Fellowship Program and China Postdoctoral Science Foundation (GZC20241040, 2024M752007), Fundamental and Interdisciplinary Disciplines Breakthrough Plan of the Ministry of Education of China (JYB2025XDXM611), the Fundamental Research Funds for the Central Universities, Shanghai Frontiers Science Center of Cellular Homeostasis and Human Diseases.

Abstract

Hematopoietic stem cells (HSCs) sustain physiological hematopoiesis by generating all hematopoietic cells. However, the connection between HSC stemness/activities and organismal lifespan, especially under stress, remains incompletely understood. We previously revealed a unique mutation at the SUMOylation site of SIRT3 (lysine 223 to arginine, K223R) that could enhance its deacetylase activity. Here, using *Sirt3*-K223R transgenic mice, we demonstrate that SIRT3 deSUMOylation promotes HSC self-renewal, inhibits myeloid differentiation, and delays HSC senescence under multiple stress conditions. Notably, these effects are associated with extended lifespan in mice, though the underlying link between preserved HSC function and lifespan extension needs further investigation. Mechanistically, SIRT3 regulates mitochondrial metabolic activity and promotes the deacetylation of H3K9 and H3K27. This epigenetic modification attenuates the RIG-I signaling pathway by downregulating DHX58 and IRF7, sustaining HSC activities. Our study uncovers a unique SIRT3-DHX58-IRF7 axis that sustains HSC activities to delay organismal aging under stress, providing insights into potential anti-aging strategies targeting hematopoietic homeostasis.

Key words: hematopoietic stem cells, HSC activities, aging, SIRT3, deSUMOylation

Introduction

Throughout the aging process, the functionality of various organs and the stemness/activity of adult stem cells (e.g., hematopoietic stem cells, HSCs) undergo significant deterioration[1]. Aging, as well as other stress conditions (i.e., chemotherapy, irradiation), usually affects the cell fate decisions of different types of adult stem cells[2]. HSCs, characterized by their unique ability to self-renew and differentiate into all hematopoietic lineages, play a pivotal role in the aging of both the entire hematopoietic system and other important organs[3, 4]. The aging of HSCs has been linked to multiple hematological dysfunctions, including lymphoid deficiency, diminished immune competence, increased DNA damage, and leukemia[5-7]. HSC aging is a key driver of systemic aging in the hematopoietic system and broader organismal homeostasis[4, 8], highlighting the importance of understanding HSC aging for health and longevity. Elucidating the molecular mechanisms underlying HSC aging is crucial for combating aging-related disorders and advancing therapeutic strategies.

Sirtuins, a family of NAD^+-dependent protein deacetylases, play a crucial role in regulating various aging-related cellular processes, particularly under stress conditions[9, 10]. For instance, SIRT2 enhances the self-renewal ability of HSCs during aging by inhibiting NLRP3 inflammasome activation[11], SIRT6 maintains HSC homeostasis by inhibiting the Wnt signaling pathway[12], and SIRT7 reinforces the regenerative capacity of HSCs during aging by regulating the mitochondrial unfolded protein response (UPRmt)[13]. Among sirtuins, SIRT3 is of particular interest due to its mitochondrial localization and role in metabolic regulation. Notably, inhibition of SIRT3 is closely associated with the progression of age-related diseases, including cancer, cardiovascular diseases, and neurodegenerative diseases[14, 15]. Consistently, *Sirt3*-deficient mice exhibit a shortened lifespan[16] , whereas elevated SIRT3 expression

under calorie restriction conditions can mitigate oxidative damage and prevent age-related diseases[17]. These findings underscore the protective role of SIRT3 in organismal aging. However, the specific mechanisms by which SIRT3 regulates HSC aging and fate determination remain elusive.

SIRT3 is a known target of SUMOylation (Small Ubiquitin-like Modifier), a post-translational modification that negatively regulates its deacetylase activity. The murine *Sirt3*-K223R mutant prevents SIRT3 SUMOylation and renders it constitutively active[17]. However, the role of SIRT3 SUMOylation in HSC fate determination and aging has not been established. Specifically, how constitutive SIRT3 activation affects HSC fate determination under stress conditions, and whether enhanced HSC activity through SIRT3 activation directly contributes to extended lifespan, remain unknown.

In this study, we investigated the role of SIRT3 in HSC activities and its direct impact on mouse lifespan using *Sirt3*-K223R mutant mice (*Sirt3*-KR) with constitutively active SIRT3, especially under stress conditions such as aging, serial transplantation and chemotherapy.

Methods

Aging Model and Competitive Transplantation Assays

To investigate the role of SIRT3 in extending recipient lifespan, 2×10^6 BM cells from *Sirt3*-WT or *Sirt3*-KR donor mice were transplanted into lethally irradiated CD45.2 recipient mice. Body weight was monitored every 4 weeks from 12 weeks post-transplantation, and post-transplant survival of the recipient mice was meticulously monitored and documented. At 12 months post-transplantation, the frequency of $Lin^-Sca\text{-}1^+c\text{-}Kit^+CD34^-CD135^-$ long-term hematopoietic stem cells (LT-HSCs) in bone marrow (BM) and myeloid ($Mac\text{-}1^+Gr\text{-}1^+$), B ($B220^+$), and T ($CD3e^+$) lineage

chimerism in peripheral blood (PB) were quantified by flow cytometry. To assess the functional activity of HSCs from primary recipients, 2×10^5 CD45.2$^+$ donor BM cells (*Sirt3*-WT or *Sirt3*-KR) were transplanted with 2×10^5 CD45.1$^+$ competitor cells into lethally irradiated CD45.1 mice via retroorbital injection. PB chimerism (CD45.2$^+$) was analyzed at 3-16 weeks post-transplantation. At 16 weeks, donor-derived myeloid (Mac-1$^+$Gr-1$^+$), B (B220$^+$), and T (CD3e$^+$) lineage subsets were further examined using anti-CD45.1, CD45.2, Mac-1, Gr-1, B220, and CD3e antibodies. All animal experiments were approved by the Institutional Animal Care and Use Committee (IACUC) of Shanghai Jiao Tong University School of Medicine and performed in accordance with the Guidelines for Animal Care.

Metabolic Analysis

Oxygen consumption rate (OCR) was determined in *Sirt3*-WT and *Sirt3*-KR hematopoietic cells using the XF Cell Mito Stress Test Kit (Seahorse #103015-100) on a Seahorse XF96 analyzer, following the manufacturer's instructions. In brief, for OCR measurement, 3×10^5 *Sirt3*-WT or *Sirt3*-KR hematopoietic cells were seeded into 96-well plates pre-coated with BD Cell-Tak (BD Biosciences). The cells were maintained in XF basic medium supplemented with 10 mM glucose, 1 mM sodium pyruvate and 2 mM glutamine (pH 7.4 at 37 °C). The injection port A on the sensor cartridge was loaded with 1.5 μM oligomycin, 2 μM of FCCP was loaded into port B and 0.5 μM rotenone/antimycin A was loaded into port C. ATP level was analyzed using the ATP Bioluminescence Assay Kit HS II (Roche) according to the manufacturer's protocol, and data were normalized to cell count.

Functional, Biochemical, and Molecular assays

Competitive repopulation assays, flow cytometric analyses (including cell cycle, apoptosis, mitochondrial membrane potential, and ROS detection), senescence-associated β-galactosidase staining, immunofluorescence staining, RNA sequencing and quantitative RT-PCR, luciferase reporter assays, chromatin immunoprecipitation (ChIP) assays, western blotting, and cleavage under targets and tagmentation (CUT&Tag) analyses were performed as detailed in Supplemental Methods. Primer sequences for genotyping, quantitative RT-PCR (qRT-PCR), dual-luciferase reporter assay, and CUT&Tag are listed in Table S1.

Results

SIRT3 constitutive activation inhibits HSC aging under stress conditions and markedly extends the overall lifespan of mice

We utilized a murine model with a constitutive activation of SIRT3 introduced by CRISPR-Cas9 targeting the SUMOylation site at lysine 223 (*Sirt3*-K223R or *Sirt3*-KR[17]) to investigate the role of SIRT3 in HSCs (Figure S1A). We explored the impact of the SIRT3 SUMOylation site mutation on HSC aging by assessing the multilineage differentiation potential, HSC frequency, the proportion of cells positive for β-galactosidase (SA-β-Gal) staining, and the expression levels of the senescence-associated genes *p16* (INK4a) and *p21* (CIP1). Aged (24-month-old) WT mice showed significantly higher HSC frequency than young (6-month-old) WT mice, whereas HSC frequency in *Sirt3*-KR mice remained stable with age (Figure S1B). Aged *Sirt3*-KR mice displayed attenuated myeloid skewing, with no significant differences observed in young mice (Figure S1C). Notably, SA-β-Gal positivity in Lin^- progenitor cells and HSCs was robustly reduced in both young and aged *Sirt3*-KR mice relative to WT controls (Figure S1D, E), accompanied by decreased expression of *p16* and *p21* in

HSCs (Figure 1A). These findings demonstrate that constitutive activation of SIRT3 attenuates HSC senescence during aging.

Aged HSCs are known to exhibit impaired repopulation capacity and a myeloid differentiation bias[18, 19]. However, to what extent the aged HSCs contribute to the lifespan remains largely unknown. To address this, we conducted bone marrow transplantation (BMT) with total BM cells from *Sirt3*-KR or *Sirt3*-WT donor mice into lethally irradiated syngeneic recipient mice to evaluate HSC frequency, the lineage distributions, repopulation abilities and overall lifespan (Figure S1F). At 12 months post-transplantation, recipients reconstituted with *Sirt3*-KR bone marrow exhibited reduced HSC and myeloid cell frequencies, accompanied by elevated B-cell frequencies compared to WT controls (Figure 1B, C). Strikingly, the median lifespan of recipients engrafted with *Sirt3*-KR BM cells was markedly extended (432 days vs. 382 days, Figure 1D). Body weight analysis revealed that weight gain gradually slowed by 42 weeks post-transplantation, indicating the onset of senescence (Figure S1G). Terminal-stage animals showed significant weight loss (Figure S1H), accompanied by decreased HSC frequency (Figure S1I) and a strong myeloid differentiation bias (Figure S1J). These observations collectively suggest that improved HSC function may delay age-related hematopoietic decline and contribute to extended lifespan.

We further performed secondary competitive BMT assays using cells from the primary recipients at 12 months post-transplantation and showed that *Sirt3*-KR HSCs exhibited enhanced repopulating capabilities (Figure 1E) and a reduced tendency toward myeloid lineage differentiation (Figure 1F) as compared with *Sirt3*-WT HSCs. Competitive transplantation demonstrated that aged *Sirt3*-KR HSCs exhibited markedly higher donor-derived repopulation capacity than aged WT HSCs (Figure

S1K). Collectively, these findings indicate that deSUMOylation of SIRT3 sustains HSC function, delays HSC aging, and contributes to extended lifespan in recipient mice.

The deSUMOylation of SIRT3 preserves HSC self-renewal under other stress conditions

To further examine whether SIRT3 deSUMOylation also preserves HSC self-renewal under additional stress, we performed serial transplantation assays (Figure S2A). Although the engraftment levels were similar between *Sirt3*-KR and *Sirt3*-WT donor HSCs after primary transplantation (Figure S2B), donor cells derived from *Sirt3*-KR mice presented better repopulation at 8, 12, and 16 weeks after secondary transplantation (Figure 2A). The BM reconstitution ability of *Sirt3*-KR cells dramatically exceeded that of *Sirt3*-WT cells after tertiary and quaternary transplantation (Figure 2B, C). Meanwhile, no significant differences in lineage differentiation were observed between *Sirt3*-WT and *Sirt3*-KR donor cells after primary transplantation (Figure S2C). Interestingly, lymphoid reconstitution from *Sirt3*-KR donor cells gradually increased after secondary, tertiary and quaternary transplants (Figure S2D, E; Figure 2D), consistent with the delayed aging phenotype of HSCs.

We also dissected the influence of SIRT3 on HSC cell cycle kinetics and apoptosis under stress conditions and demonstrated that SIRT3 could suppress HSC apoptosis as evaluated by the flow cytometric analysis at 16 weeks post-transplantation (Figure S2F). An increased frequency of HSCs in G0 phase was observed in *Sirt3*-KR mice compared with *Sirt3*-WT mice (Figure S2G). After secondary transplantation, donor HSCs from *Sirt3*-KR mice displayed similar inhibition of apoptosis and enhancement of quiescence (Figure S2H, I). These findings indicate that the mutation in the SIRT3

SUMOylation site inhibits HSC apoptosis and enhances quiescence under stress conditions, highlighting the importance of SIRT3 in different HSC fates.

We further tested the impact of SIRT3 on HSC fates using other stress conditions, including *in vitro* culture and chemotherapeutic treatment. Primary LT-HSCs were cultured *ex vivo* and then transplanted into recipient mice. After 8 days of culture, the number and frequency of immunophenotypic $Lin^{-}Sca\text{-}1^{+}c\text{-}Kit^{+}$ (LSK) cells were significantly increased in *Sirt3*-KR-derived HSCs (Figure S2J, K). More importantly, recipient mice showed an improved reconstitution ability and increased lymphoid differentiation with *Sirt3*-KR donor cells (Figure 2E; Figure S2L, M). We continued to treat *Sirt3*-KR mice with two chemotherapeutic agents, including 5-fluorouracil (5-FU) or cyclophosphamide (CTX), to evaluate the HSC activities by competitive transplantation assays. Compared with that in *Sirt3*-WT HSCs, the frequency of HSCs in *Sirt3*-KR mice was significantly increased after the 5-FU treatment (Figure S2N). Moreover, PB chimerism from *Sirt3*-WT donors was notably decreased compared with that from *Sirt3*-KR donors at 16 weeks post-transplantation (Figure S2O). After CTX treatment, the frequency of HSCs in *Sirt3*-KR mice was significantly higher than that in *Sirt3*-WT mice (Figure S2P). More importantly, HSCs from *Sirt3*-KR mice exhibited enhanced repopulation abilities and lymphoid differentiation potential after CTX treatment (Figure 2F; Figure S2Q). Collectively, these findings show that HSCs from *Sirt3*-KR mice exhibit enhanced self-renewal and delayed aging under different stress conditions.

SIRT3 sustains HSC activities and delays aging by regulating inflammation-associated pathways

To elucidate the molecular mechanisms by which SIRT3 deSUMOylation regulates HSC function and aging, we performed RNA-sequencing using HSCs from *Sirt3*-WT and *Sirt3*-KR mice. A total of 593 differentially expressed genes (DEGs) were identified, including 305 upregulated and 288 downregulated genes in *Sirt3*-KR HSCs, which were highly enriched in immune- and inflammation-related pathways (Figure S3A, B). Several immune related regulators, including *Mx1*, *Mx2*, *Irf7*, *Oas1g*, *Oasl2*, *Dhx58*, *Oas2*, *Ifit1* and *Ifi44* were significantly reduced in *Sirt3*-KR HSCs (Figure S3C). Regarding that SIRT3 is also reported to modulate gene expression by modifying the chromatin status through the deacetylation of H3K9 and H3K27[20], we further performed the CUT&Tag analysis. The results revealed markedly lower enrichment of H3K9ac and H3K27ac in *Sirt3*-KR HSCs and hematopoietic stem/progenitor cells (HSPCs) compared with *Sirt3*-WT cells (Figure 3A; Figure S3D). Western blot analyses also demonstrated decreased acetylation of H3K9 and H3K27 in *Sirt3*-KR cells (Figure S3E).

Conjoint analysis of RNA-seq and CUT&Tag data identified 90 commonly downregulated genes in *Sirt3*-KR HSCs, which were strongly enriched in the RIG-I-like receptor signaling pathway, including *Dhx58*, *Gbp5*, *Irf7*, *Mx1*, *Trim30a* and *Ifi44* (Figure 3B; Figure S3F). RT-qPCR further verified the reduced expression of these genes in *Sirt3*-KR HSCs (Figure 3C). Given that *Dhx58* encodes a RIG-I-like receptor that modulates interferon and pro-inflammatory cytokine expression via *Irf7*[21, 22], we hypothesized that SIRT3 deSUMOylation may suppress the RIG-I-like receptor signaling pathway.

CUT&Tag data revealed an enrichment of the *Dhx58* and *Irf7* genes in *Sirt3*-WT HSCs and HSPCs, with the higher transcript abundance and increased levels of the active histone marks H3K9ac and H3K27ac (Figure 3D; Figure S4A). ChIP-qPCR

revealed a greater enrichment of acetylated H3K27 and H3K9 at the *Dhx58* or *Irf7* promoter in *Sirt3*-WT LT-HSCs than in *Sirt3*-KR ones (Figure 3E, F; Figure S4B, C). These findings suggest that decreased H3K9ac and H3K27ac levels are involved in the transcriptional repression of the *Dhx58* and *Irf7* genes upon SIRT3 deSUMOylation.

It has been reported that SIRT3 governs a mitochondrial protective program in stem cells and prevents stem cell aging[23]. Moreover, mitochondrial dysfunction can trigger cGAS-STING activation[24]. We speculated that the SUMOylation site mutation of SIRT3 may prevent the activation of the cGAS-STING pathway. Indeed, we found that *cGas* expression level was downregulated in *Sirt3*-KR mice, with no significant changes in *Sting*, *Tbk1* and *Irf3* expression according to RNA-Seq (Figure S4D). However, immunofluorescence staining and western blotting further confirmed that mutation of the SIRT3 SUMOylation site reduced STING and phosphorylated TBK1 (p-TBK1) levels (Figure S4E, F). Cytosolic mtDNA levels (*mtND1*, *mtCOX2*) and mitochondrial ROS (MitoSOX) were significantly lower in *Sirt3*-KR HSPCs compared with WT controls (Figure S4G-I). These results indicate that SIRT3 deSUMOylation plays a role in inhibiting the activation of cGAS-STING signaling pathway.

SIRT3 promotes HSC self-renewal and delays HSC aging through the downregulation of DHX58

We then evaluated how DHX58 regulates HSC self-renewal and aging and found that the overexpression of *Dhx58* in *Sirt3*-KR HSCs significantly impaired the BM reconstitution capacity of *Sirt3*-KR cells (Figure S5A; Figure 4A) and reversed the tendency to myeloid differentiation (Figure 4B). Meanwhile, we found that *Dhx58* overexpression in *Sirt3*-KR HSCs increased the proportion of SA-β-Gal-positive cells (Figure S5B; Figure 4C) and upregulated the expression of the senescence-associated

marker genes *p16* and *p21* (Figure 4D). These results indicate that SIRT3 suppresses DHX58 expression to preserve HSC activities and delays HSC aging.

Senescent cells secrete a plethora of growth factors, cytokines, and proteases, contributing to a senescence-associated secretory phenotype (SASP). Notably, IL-1β, and IL-6 are known to trigger cellular senescence[25, 26]. We speculated that the secretion of IL-1β and IL-6 could lead to HSC senescence in a paracrine manner. Indeed, the addition of IL-1β and IL-6 to the culture medium promoted 32D cells (a myeloid progenitor cell line) to enter senescence process in a dose-dependent manner (Figure S5C, D). Consistently, *Dhx58*-overexpressing 32D cells (32D-*Dhx58*-OE) presented increased expression of *Il-1β* and *Il-6* (Figure S5E, F), elevated levels of the DNA damage response (DDR) factor γ-H2A.X (Figure S5G, H), and a higher proportion of senescent cells positive for β-galactosidase staining (Figure S5I, J). *Sirt3*-KR HSCs showed significantly reduced *Il-1β* and *Il-6* expression compared with *Sirt3*-WT HSCs. Notably, this reduction was rescued by *Dhx58* overexpression (Figure 4E). Collectively, these findings demonstrate that SIRT3 inhibits HSC senescence and SASP by suppressing DHX58.

IRF7 serves as a DHX58 downstream target to regulate HSC stemness and aging

DHX58 acts as a cofactor to coordinate the RIG-1 and MDA5 function in RNA recognition and activates downstream IRF7 signaling to promote the secretion of inflammatory factors, such as IL-6 and INF-γ[27]. We noticed that *Irf7* expression was significantly reduced in *Sirt3*-KR HSCs (Figure 3C), suggesting IRF7 may act as a downstream effector of SIRT3. Indeed, the overexpression of *Irf7* markedly reduced the BM reconstitution capacity of *Sirt3*-KR HSCs but exerted no significant effect on *Sirt3*-WT HSCs (Figure S6A; Figure 5A). The overexpression of *Irf7* also led to a

decrease in B-lymphoid differentiation and an increase in myeloid differentiation (Figure 5B). Furthermore, *Irf7* overexpression accelerated senescence of *Sirt3*-KR HSCs, as shown by elevated SA-β-galactosidase activity and increased expression of *p16*, *p21*, *Il-1β*, and *Il-6* (Figure 5C, D; Figure S6B, C). These results show that, similarly to *Dhx58*, *Irf7* overexpression triggers cellular senescence, suggesting that it serves as a critical downstream of SIRT3.

We then investigated how SIRT3 regulates HSC activities, including enhanced self-renewal and reduced tendency to myeloid cells. Indeed, RNA-sequencing data showed that genes related to HSC self-renewal (*Hoxb4*, *Bmi1*, *Mllt3* and *Gata2*) were significantly upregulated in *Sirt3*-KR HSCs, whereas myeloid differentiation related genes (*Pu.1* and *Cebpa*) were downregulated. Additionally, lymphoid differentiation related genes (*Ikaros, E2a, Sox4* and *Bcl11a*) were upregulated in *Sirt3*-KR HSCs (Figure S6D). Quantitative RT-PCR assays further confirmed that *Hoxb4*, *Mllt3* and *Gata2* were significantly upregulated, whereas *Pu.1*, *Gata1* and *Cebpa* were significantly downregulated. Additionally, *Pax5*, *Ebf1*, *E2a*, *Sox4* and *Bcl11a* were notably increased in *Sirt3*-KR HSCs (Figure S6E).

We next examined how IRF7 mediates the effects of SIRT3 on HSC self-renewal and differentiation. We found that *Irf7* overexpression inhibited the expression of key self-renewal- and B-cell differentiation-related genes, including *Hoxb4*, *Mllt3*, *Gata2*, *Pax5*, *Ebf1*, *E2a* and *Sox4*, while promoting the expression of the myeloid differentiation-related genes *Pu.1* and *Gata1* (Figure S6F, G). Dual-luciferase reporter assay showed that IRF7 could repress the transcription of *Gata2* and *Mllt3* while transactivating *Pu.1* and *Gata1* expression (Figure S6H, I; Figure 5E). ChIP-PCR analysis further confirmed direct binding of IRF7 to the promoters of these genes (Figure S6J-M). Overall, these results suggest that SIRT3 can inhibit the DHX58-IRF7

signaling by regulating histone modifications, thereby increasing self-renewal and inhibiting senescence in HSCs.

SIRT3 enhances mitochondrial metabolism and α-KG generation in HSCs

SIRT3 has been reported to play important roles in mitochondrial metabolism to further initiate downstream signaling pathway[17, 28]. To understand how SIRT3 regulates DHX58-IRF7 signaling, we then analyzed the respiratory status of *Sirt3*-KR and showed that *Sirt3*-KR HSCs exhibited significantly higher OCR, ATP levels, and mitochondrial membrane potential than *Sirt3*-WT counterparts (Figure 6A-C). Consistently, we also observed a notable increased mitochondrial count (Figure S7A, B) and a larger mitochondrial area and greater quantity in *Sirt3*-KR HSCs by electron microscopy (Figure 6D).

We previously established a metabolic SoNar sensor that could sensitively and specifically detect the ratio of NADH and NAD^+ both *in vitro* and *in vivo*. The higher/lower SoNar ratio (NADH/NAD^+) reflected the higher/lower activities of glycolysis and tricarboxylic acid cycle (TCA), respectively[29, 30]. While the iNap sensor is capable of accurately detecting the levels of reduced NADPH[31]. We further generated *Sirt3*-KR/SoNar and *Sirt3*-KR/iNap double transgenic mice and demonstrated that *Sirt3*-KR HSCs had much higher levels of TCA (lower SoNar ratio, Figure S7C, D), and greater NADPH levels (higher iNap ratio, Figure S7E, F) than those of WT controls. The increased NADPH levels likely contribute to the markedly reduced mitochondrial ROS levels observed in *Sirt3*-KR HSCs (Figure 6E), strengthening their antioxidant capacity. Notably, α-KG levels were increased by 1.5-2-fold in *Sirt3*-KR HSCs compared to WT controls, a phenomenon consistently observed in both young

(2-month-old) and aged (20-month-old) mice (Figure 6F). This is consistent with reports that α-KG declines with age and that its homeostasis supports longevity[32, 33].

Consistently, RT-qPCR confirmed that genes involved in antioxidant defense (e.g., *Sod1*, *Sod2*, *Prdx1*, *Gpx1*) and oxidative phosphorylation (e.g., *Mdh2*, *Idh2*, *Aco2*) were upregulated in *Sirt3*-KR HSCs, while pro-oxidant genes (e.g., *Glrx2*, *Nox2*) were downregulated. Notably, among genes involved in oxidative phosphorylation, *Idh2* showed the highest expression level (Figure S7G). IDH2 catalyzes the conversion of isocitrate to α-KG with concomitant NADPH production, indicating that IDH2 may play an important role in regulating histone deacetylation in *Sirt3*-KR HSCs. Collectively, these findings demonstrate that SIRT3 deSUMOylation enhances mitochondrial metabolism, boosts antioxidant capacity, and promotes α-KG generation, which in turn drives epigenetic repression of the DHX58-IRF7 axis to sustain HSC function and delay aging (Figure 7). These observations establish a mechanistic link between adult stem cell homeostasis and organismal lifespan under stress, and provide a theoretical framework for developing aging-delaying interventions.

Discussion

The senescence of HSCs is considered a key factor leading to the dysregulation and aging of the entire hematopoietic system, as well as other organismal disorders. Sirtuins regulate a variety of cellular responses, including DNA damage repair, telomere maintenance, and metabolism[34]. SIRT2, SIRT6, and SIRT7 exert significant effects on the regulation of HSC homeostasis and aging[11-13]. Using a *Sirt3*-K223R mouse model, we demonstrated that SIRT3 deSUMOylation enhances HSC self-renewal capacity and maintains lineage-balanced differentiation through the DHX58-IRF7 signaling, ultimately prolonging lifespan in this transgenic model. Given that IRF7 inhibitors are

in clinical trials for autoimmune diseases[35], our findings suggest repurposing these compounds to ameliorate myeloid skewing in elderly patients. This effect may translate to reduced frailty and hematologic malignancy risk in elderly humans, highlighting the potential of targeting SIRT3 for improving HSC function in age-related BM disorders.

Previous studies have linked SIRT3 to cellular senescence and age-related diseases[14, 36, 37], and SIRT3 deletion was reported to shorten mouse lifespan[16]. However, whether specific adult stem cell populations such as HSCs contribute to organismal longevity remains poorly defined. Here, we found that HSCs from 24-month-old *Sirt3*-KR mice presented a reduced proportion of senescent cells and downregulated expression of the senescence-associated genes of *p16* and *p21*. These findings suggest that SIRT3 deSUMOylation inhibits HSC aging, and this protection correlates with lifespan extension in *Sirt3*-KR model. Whether HSC aging directly contributes to organismal lifespan remains to be confirmed.

Mitochondria play a central role in HSC maintenance, stress response, and aging through metabolic and epigenetic regulation[38]. Metabolites, such as acetyl-CoA, α-KG, and ROS, are crucial for enzymes that modify the chromatin structure to affect gene expression[39, 40]. SIRT3 is indispensable for maintaining mitochondrial homeostasis by regulating metabolic activity through multiple substrate proteins[41], and this function has attracted intense interest in senescence and aging research[15, 42]. Notably, we observed that *Sirt3*-KR HSCs displayed elevated mitochondrial activity (Figure 6) and enhanced quiescence (Figure S2G), which appears contradictory to the general model that quiescent HSCs rely on glycolysis. Future studies should dissect whether this reflects a unique metabolic state in stress-resistant HSCs (e.g., high mitochondrial quality but low respiratory rate).

The RIG-I signaling pathway has emerged as a key regulator of aging, linking DNA damage to inflammatory senescence[43]. Several inflammatory factors, such as IL-1, IL-6, IL-11, CCL4 and IL-8, are known to promote the progression of senescence[25, 26, 44, 45]. Interestingly, our study demonstrated that SIRT3 deSUMOylation leads to reduced secretion of IL-1β and IL-6. However, the cellular source of these cytokines (e.g., HSCs or other hematopoietic cells) and their direct impact on lifespan require further study. Consistent with previous studies showing that inhibition of IL-1 signaling or administration of anti-IL-11 antibodies can attenuate HSC senescence and promote longevity[45, 46], our findings highlight the potential of targeting inflammatory pathways as a strategy to delay aging. Additionally, SIRT3 mitigates senescence via cGAS-STING suppression[47] , and we observed downregulated cGAS, STING, TBK1 in *Sirt3*-KR HSCs. However, the extent to which cGAS-STING signaling contributing to the lifespan remains to be elucidated.

We previously demonstrated that SIRT3 deSUMOylation is specifically regulated by the AMPK-SENP1 pathway[48], which provides a basis for further screening and exploring the role of SIRT3 SUMOylation agonists or antagonists in HSC fate determination. In future, we will focus on exploring the potential of small-molecule compounds and gene-therapeutic strategies that precisely target this signaling axis. Importantly, SUMOylation sites are conserved in human SIRT3, and mutation of these sites activates SIRT3 deacetylase activity[17]. Investigating the role of SIRT3 SUMOylation in human HSC aging will be crucial for translating these findings into lifespan-extending interventions.

In conclusion, SIRT3 deSUMOylation serves as a key regulator of HSC stress resistance, acting via the DHX58-IRF7 axis and mitochondrial metabolism. These findings advance our understanding of HSC functional maintenance under stress and

provide a mechanistic basis for developing strategies to preserve hematopoietic homeostasis during aging.

References

1. Campisi J, Kapahi P, Lithgow GJ, Melow S, Newman JC, Verdin E. From discoveries in ageing research to therapeutics for healthy ageing. Nature. 2019;571(7764):183-192.
2. Kuijk E, Kranenburg O, Cuppen E, Van Hoek A. Common anti-cancer therapies induce somatic mutations in stem cells of healthy tissue. Nature Commun. 2022;13(1):5915.
3. Rodriguez-Fraticelli AE, Wolock SL, Weinreb CS, et al. Clonal analysis of lineage fate in native haematopoiesis. Nature. 2018;553(7687):212-216.
4. Zhang B, Lee DE, Trapp A, et al. Multi-omic rejuvenation and life span extension on exposure to youthful circulation. Nat Aging. 2023;3(8):948-964.
5. Ross JB, Myers LM, Noh JJ, et al. Depleting myeloid-biased haematopoietic stem cells rejuvenates aged immunity. Nature. 2024;628(8006):162-170.
6. Mejia-Ramirez E, Florian MC. Understanding intrinsic hematopoietic stem cell aging. Haematologica. 2020;105(1):22-37.
7. Liang C, Liu Z, Song M, et al. Stabilization of heterochromatin by CLOCK promotes stem cell rejuvenation and cartilage regeneration. Cell Res. 2021;31(2):187-205.
8. Kollman C, Howe CW, Anasetti C, et al. Donor characteristics as risk factors in recipients after transplantation of bone marrow from unrelated donors: the effect of donor age. Blood. 2001;98(7):2043-2051.
9. Fang Y, An N, Zhu L, et al. Autophagy-Sirt3 axis decelerates hematopoietic aging. Aging Cell. 2020;19(10):e13232.
10. Finkel T, Deng CX, Mostoslavsky R. Recent progress in the biology and physiology of sirtuins. Nature. 2009;460(7255):587-591.
11. Luo H, Mu WC, Karki R, et al. Mitochondrial Stress-Initiated Aberrant Activation of the NLRP3 Inflammasome Regulates the Functional Deterioration of Hematopoietic Stem Cell Aging. Cell Rep. 2019;26(4):945-954.e4.
12. Wang H, Diao D, Shi Z, et al. SIRT6 Controls Hematopoietic Stem Cell Homeostasis through Epigenetic Regulation of Wnt Signaling. Cell Stem Cell. 2016;18(4):495-507.
13. Mohrin M, Shin J, Liu Y, et al. Stem cell aging. A mitochondrial UPR-mediated metabolic checkpoint regulates hematopoietic stem cell aging. Science. 2015;347(6228):1374-1377.
14. McDonnell E, Peterson BS, Bomze HM, et al. SIRT3 regulates progression and development of diseases of aging. Trends Endocrinol Metab. 2015;26(9):486-492.
15. Brown K, Xie S, Qiu X, et al. SIRT3 reverses aging-associated degeneration. Cell Rep. 2013;3(2):319-327.
16. Benigni A, Cassis P, Conti S, et al. Sirt3 Deficiency Shortens Life Span and Impairs Cardiac Mitochondrial Function Rescued by Opa1 Gene Transfer. Antioxid Redox Signal. 2019;31(17):1255-1271.
17. Wang T, Cao Y, Zheng Q, et al. SENP1-Sirt3 Signaling Controls Mitochondrial Protein Acetylation and Metabolism. Mol Cell. 2019;75(4):823-834.e5.
18. de Haan G, Lazare SS. Aging of hematopoietic stem cells. Blood. 2018;131(5):479-487.
19. DeGregori J. Aging, inflammation, and HSC. Blood. 2020;136(2):153-154.

20. Palomer X, Román-Azcona MS, Pizarro-Delgado J, et al. SIRT3-mediated inhibition of FOS through histone H3 deacetylation prevents cardiac fibrosis and inflammation. Signal Transduct Target Ther. 2020;5(1):14.
21. Lefkopoulos S, Polyzou A, Derecka M, et al. Repetitive Elements Trigger RIG-I-like Receptor Signaling that Regulates the Emergence of Hematopoietic Stem and Progenitor Cells. Immunity. 2020;53(5):934-951.e9.
22. Xiao Z, Chen H, Xu N, Chen Y, Wang S, Xu X. MATR3 promotes liver cancer progression by suppressing DHX58-mediated type I interferon response. Cancer Lett. 2024;604:217231.
23. Jiang DQ, Wang Y, Li MX, et al. SIRT3 in Neural Stem Cells Attenuates Microglia Activation-Induced Oxidative Stress Injury Through Mitochondrial Pathway. Front Cell Neurosci. 2017;11:7.
24. Domizio JD, Gulen MF, Saidoune F, et al. The cGAS-STING pathway drives type I IFN immunopathology in COVID-19. Nature. 2022;603(7899):145-151.
25. Caiado F, Manz MG. IL-1 in aging and pathologies of hematopoietic stem cells. Blood. 2024;144(4):368-377.
26. Kuilman T, Michaloglou C, Vredeveld LC, et al. Oncogene-induced senescence relayed by an interleukin-dependent inflammatory network. Cell. 2008;133(6):1019-1031.
27. Rehwinkel J, Gack MU. RIG-I-like receptors: their regulation and roles in RNA sensing. Nat Rev Immunol. 2020;20(9):537-551.
28. Peng F, Liao M, Jin W, et al. 2-APQC, a small-molecule activator of Sirtuin-3 (SIRT3), alleviates myocardial hypertrophy and fibrosis by regulating mitochondrial homeostasis. Signal Transduct Target Ther. 2024;9(1):133.
29. Gu H, Chen C, Hao X, et al. MDH1-mediated malate-aspartate NADH shuttle maintains the activity levels of fetal liver hematopoietic stem cells. Blood. 2020;136(5):553-571.
30. Hao X, Gu H, Chen C, et al. Metabolic Imaging Reveals a Unique Preference of Symmetric Cell Division and Homing of Leukemia-Initiating Cells in an Endosteal Niche. Cell Metab. 2019;29(4):950-965.e6.
31. Chen C, Lai X, Zhang Y, et al. NADPH metabolism determines the leukemogenic capacity and drug resistance of AML cells. Cell Rep. 2022;39(1):110607.
32. Chin RM, Fu X, Pai MY, et al. The metabolite alpha-ketoglutarate extends lifespan by inhibiting ATP synthase and TOR. Nature. 2014;510(7505):397-401.
33. Lee I, Piao S, Kim S, et al. IDH2 Deficiency Promotes Endothelial Senescence by Eliciting miR-34b/c-Mediated Suppression of Mitophagy and Increased ROS Production. Antioxidants (Basel). 2023;12(3):585.
34. Houtkooper RH, Pirinen E, Auwerx J. Sirtuins as regulators of metabolism and healthspan. Nat Rev Mol Cell Biol. 2012;13(4):225-238.
35. Werth VP, Furie RA, Romero-Diaz J, et al. Trial of Anti-BDCA2 Antibody Litifilimab for Cutaneous Lupus Erythematosus. N Engl J Med. 2022;387(4):321-331.
36. Yang L, Wang B, Guo F, et al. FFAR4 improves the senescence of tubular epithelial cells by AMPK/SirT3 signaling in acute kidney injury. Signal Transduct Target Ther. 2022;7(1):384.
37. Zhang J, Xiang H, Liu J, Chen Y, He R-R, Liu B. Mitochondrial Sirtuin 3: New emerging biological function and therapeutic target. Theranostics. 2020;10(18):8315-8342.

38. Chandel NS, Jasper H, Ho TT, Passegué E. Metabolic regulation of stem cell function in tissue homeostasis and organismal ageing. Nat Cell Biol. 2016;18(8):823-832.
39. Fu ZW, Li JH, Feng YR, Yuan X, Lu Y-T. The metabolite methylglyoxal-mediated gene expression is associated with histone methylglyoxalation. Nucleic Acids Res. 2021;49(4):1886-1899.
40. Kaelin WG Jr, McKnight SL. Influence of metabolism on epigenetics and disease. Cell. 2013;153(1):56-69.
41. Yang W, Nagasawa K, Münch C, et al. Mitochondrial Sirtuin Network Reveals Dynamic SIRT3-Dependent Deacetylation in Response to Membrane Depolarization. Cell. 2016;167(4):985-1000.e21.
42. Wiley CD, Velarde MC, Lecot P, et al. Mitochondrial Dysfunction Induces Senescence with a Distinct Secretory Phenotype. Cell Metab. 2016;23(2):303-314.
43. Liu F, Wu S, Ren H, Gu J. Klotho suppresses RIG-I-mediated senescence-associated inflammation. Nat Cell Biol. 2011;13(3):254-262.
44. Chang TT, Lin LY, Chen C, Chen J-W. CCL4 contributes to aging related angiogenic insufficiency through activating oxidative stress and endothelial inflammation. Angiogenesis. 2024;27(3):475-499.
45. Widjaja AA, Lim WW, Viswanathan S, et al. Inhibition of IL-11 signalling extends mammalian healthspan and lifespan. Nature. 2024;632(8023):157-165.
46. Mitchell CA, Verovskaya EV, Calero-Nieto FJ, et al. Stromal niche inflammation mediated by IL-1 signalling is a targetable driver of haematopoietic ageing. Nat Cell Biol. 2023;25(1):30-41.
47. Zhou Q, Yi G, Chang M, et al. Activation of Sirtuin3 by honokiol ameliorates alveolar epithelial cell senescence in experimental silicosis via the cGAS-STING pathway. Redox Biol. 2024;74:103224.
48. He J, Shangguan X, Zhou W, et al. Glucose limitation activates AMPK coupled SENP1-Sirt3 signalling in mitochondria for T cell memory development. Nat Commun. 2021;12(1):4371.

Figure 1. SIRT3 activation inhibits HSC aging under stress conditions and markedly extends the overall lifespan of mice. A) The relative mRNA levels of *p16* and *p21* were measured in the HSCs of young or old *Sirt3*-WT and *Sirt3*-KR mice by quantitative RT-PCR (n=3). B) Frequencies of immunophenotypic $Lin^{-}Sca\text{-}1^{+}c\text{-}Kit^{+}CD34^{-}CD135^{-}$ LT-HSCs from recipient mice receiving *Sirt3*-WT and *Sirt3*-KR BM donor cells at 12 months after transplantation. C) The multilineage contribution of donor cells in PB was quantified at 12 months after transplantation. D) Lifespan of the recipient mice receiving *Sirt3*-WT or *Sirt3*-KR BM donor cells is shown (n=15). E) The repopulation ability of donor cells from *Sirt3*-WT and *Sirt3*-KR mice was determined by flow cytometric analysis at the indicated time points (n=5). F) The multilineage contribution of donor cells in the PB was quantified at 16 weeks after transplantation (n=5). *P<0.05, **P<0.01, ***P<0.001.

Figure 2. The deSUMOylation of SIRT3 preserves HSC self-renewal under stress conditions. A-C) The repopulation of *Sirt3*-WT and *Sirt3*-KR donor cells was measured 3 to 16 weeks after the 2^{nd} (A), 3^{rd} (B) and 4^{th} (C) transplantations (n=5). D) The multilineage differentiation of donor cells into myeloid cells ($Mac\text{-}1^{+}$ and $Gr\text{-}1^{+}$), B cells ($B220^{+}$), and T cells ($CD3^{+}$) in PB was quantitated by flow cytometry at 16 weeks after the 4^{th} transplantation (n=5). E) The repopulation ability of cultured HSCs from *Sirt3*-WT and *Sirt3*-KR mice at the indicated time points after transplantation (n=5). F) The repopulation ability of donor cells from CTX-treated *Sirt3*-WT and *Sirt3*-KR mice was determined by flow cytometric analyses at the indicated time points (n=5). *P<0.05, **P<0.01, ***P<0.001.

Figure 3. SIRT3 sustains HSC activities and delays aging by regulating inflammation-associated pathways. A) Heatmap showing CUT&Tag-seq coverage at sites with altered H3K9ac and H3K27ac modifications in *Sirt3*-KR HSCs compared

with the *Sirt3*-WT group. B) Venn diagram of matching DEGs among RNA-seq, H3K9ac CUT&Tag-seq and H3K27ac CUT&Tag-seq data. C) Relative mRNA expression of potential candidates (*Dhx58*, *Oas3*, *Irf7* and *Mx1*) in LT-HSCs purified from *Sirt3*-WT and *Sirt3*-KR mice, as measured by quantitative RT-PCR (n=3). D) Analysis of H3K9ac and H3K27ac CUT&Tag-seq at peaks in the genomic regions of DHX58 and IRF7. E) ChIP-qPCR analysis of H3K9ac or H3K27ac levels at the promoter of *Dhx58* in HSCs isolated from *Sirt3*-WT and *Sirt3*-KR mice. F) ChIP-qPCR analysis of H3K9ac or H3K27ac levels at the promoter of *Irf7* in HSCs isolated from *Sirt3*-WT and *Sirt3*-KR mice. **P<0.01, ***P<0.001.

Figure 4. SIRT3 promotes HSC self-renewal and delays HSC aging through the downregulation of DHX58. A) Quantification of HSC repopulation capacity from *Sirt3*-WT and *Sirt3*-KR mice with/without *Dhx58* overexpression (RFP^+ cells) at the indicated time points post-transplantation (n=5). B) The multilineage contribution of donor cells in PB was quantified at 16 weeks after transplantation (n=5). C) The frequencies of SA-β-Gal-expressing *Sirt3*-WT, *Sirt3*-KR, *Dhx58*-overexpressing *Sirt3*-WT and *Sirt3*-KR Lin^- cells were measured. D) The relative mRNA expression of aging-related genes *p16* and *p21* in *Sirt3*-WT, *Sirt3*-KR, *Dhx58*-overexpressing *Sirt3*-WT or *Sirt3*-KR HSCs was measured by quantitative RT-PCR (n=3). E) The relative mRNA levels of the senescence-associated secretory phenotype (SASP) factors *Il-1β* and *Il-6* were measured in *Sirt3*-WT, *Sirt3*-KR, *Dhx58*-overexpressing *Sirt3*-WT and *Sirt3*-KR HSCs via quantitative RT-PCR (n=3). *P<0.05, **P<0.01, ***P<0.001.

Figure 5. IRF7 serves as a DHX58 downstream target to regulate HSC stemness and aging. A) Quantification of HSC repopulation capacity from *Sirt3*-WT and *Sirt3*-KR mice with/without *Irf7* overexpression (RFP^+ cells) at the indicated time points post-transplantation (n=5). B) The multilineage contribution of donor cells in PB was

quantified at 16 weeks after transplantation (n=5). C) The frequencies of SA-β-Gal-expressing *Sirt3*-WT, *Sirt3*-KR, *Irf7*-overexpressing *Sirt3*-WT and *Sirt3*-KR Lin^- cells were measured. D) The relative mRNA expression levels of aging-related genes (*p16* and *p21*) in *Sirt3*-WT, *Sirt3*-KR, *Irf7*-overexpressing *Sirt3*-WT or *Sirt3*-KR HSCs were measured by quantitative RT-PCR (n=3). E) A luciferase reporter assay was performed to evaluate the transcriptional activity of IRF7 at the promoters of *Pu.1* and *Gata1* (n=3). *P<0.05, **P<0.01, ***P<0.001.

Figure 6. SIRT3 serves as a key regulator of mitochondrial metabolism in HSCs. A) OCR was measured in *Sirt3*-WT (red) and *Sirt3*-KR (blue) HSPCs using a Seahorse XF96 analyzer under basal conditions and in response to sequential addition of 1.5 μM oligomycin, 2 μM FCCP, and 0.5 μM rotenone/antimycin A. B) ATP levels in *Sirt3*-WT and *Sirt3*-KR HSCs were measured with an ATP assay kit (n=3). C) Mean fluorescence intensity (MFI) of the TMRM in *Sirt3*-WT and *Sirt3*-KR HSCs (n=3). D) Mitochondrial morphology as well as quantitative analyses of mitochondrial area and number in HSCs from *Sirt3*-WT and *Sirt3*-KR mice were examined by transmission electron microscopy. Scale bar, 500 nm. E) Measurement of 2',7'-dichlorofluorescein diacetate (H_2DCFDA) levels in *Sirt3*-WT and *Sirt3*-KR HSCs by flow cytometry (n=3). F) Relative α-KG levels in HSCs isolated from *Sirt3*-WT and *Sirt3*-KR mice at 2 and 20 months of age (n=3). *P<0.05, **P<0.01, ***P<0.001.

Figure 7. Working model. A working model for the roles of SIRT3 in HSC activities, aging and mouse lifespan. Under stress conditions such as serial transplantation, chemotherapy or aging, the deSUMOylation of SIRT3 enhances HSC self-renewal and lymphoid differentiation potential, while suppressing HSC aging and extending lifespan. Mechanistically, deSUMOylated SIRT3, achieved by constitutive activation of the SIRT3 mutant (K223R), inhibits senescence-associated inflammatory responses

through a novel mechanism involving increased α-KG levels, which in turn suppresses the acetylation of H3K9 and H3K27. This leads to inhibition of key genes in the RIG-I signaling pathway, including DHX58 and IRF7. IRF7 induces the expression of myeloid differentiation-related genes such as *Pu.1* and *Gata1*, while repressing HSC self-renewal-related genes including *Gata2* and *Mllt3*. The SIRT3-DHX58-IRF7 signaling axis downregulates the expression of the SASP factors IL-1β and IL-6, which are critical for HSC stemness maintenance and longevity.

Figure 1

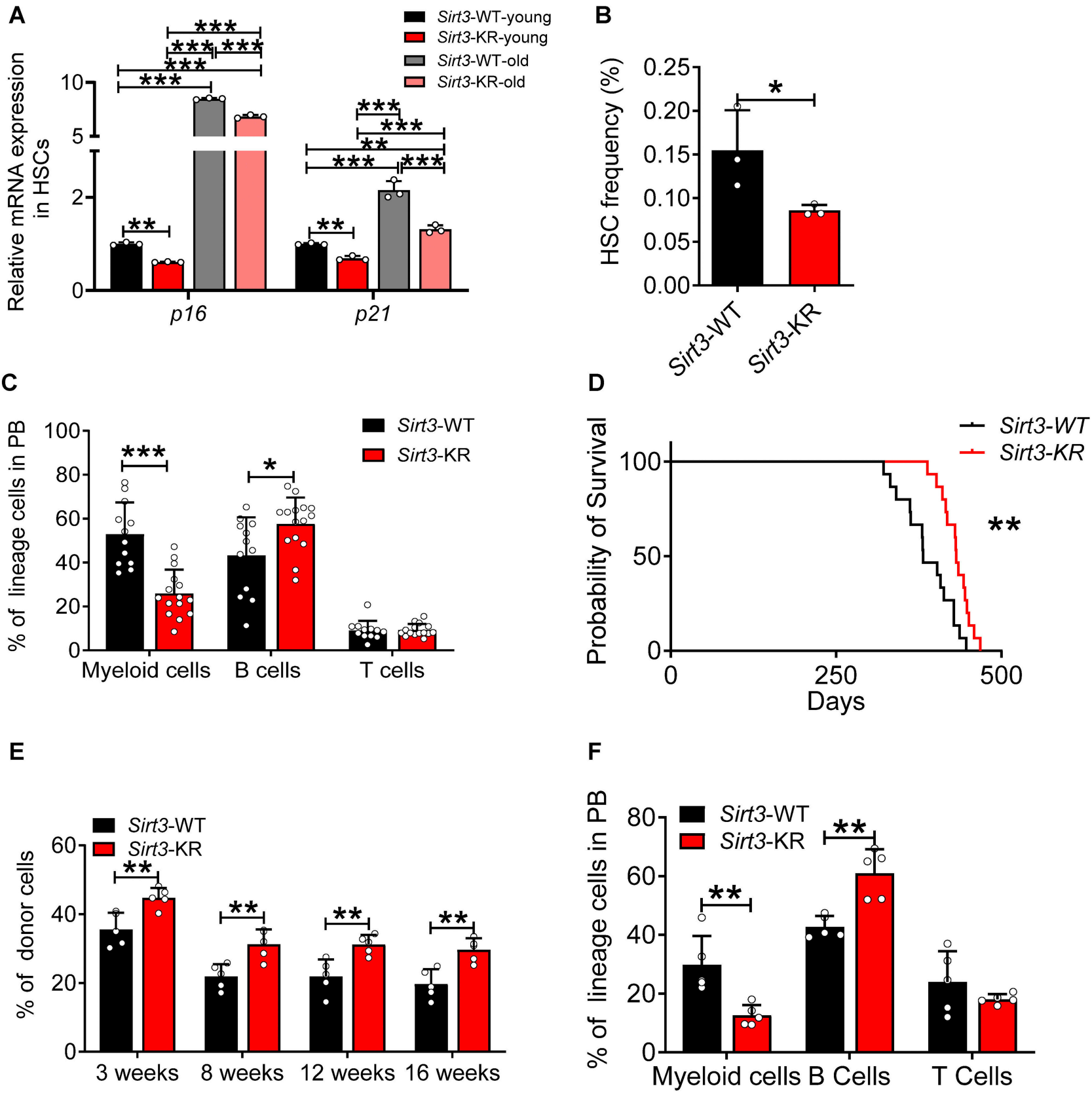
A
Sirt3-WT-young
Sirt3-KR-young
Sirt3-WT-old
Sirt3-KR-old
Relative mRNA expression in HSCs
p16
p21
B
HSC frequency (%)
Sirt3-WT
Sirt3-KR
C
Sirt3-WT
Sirt3-KR
% of lineage cells in PB
Myeloid cells
B cells
T cells
D
Sirt3-WT
Sirt3-KR
Probability of Survival
Days
E
Sirt3-WT
Sirt3-KR
% of donor cells
3 weeks
8 weeks
12 weeks
16 weeks
F
Sirt3-WT
Sirt3-KR
% of lineage cells in PB
Myeloid cells
B Cells
T Cells

Figure 2

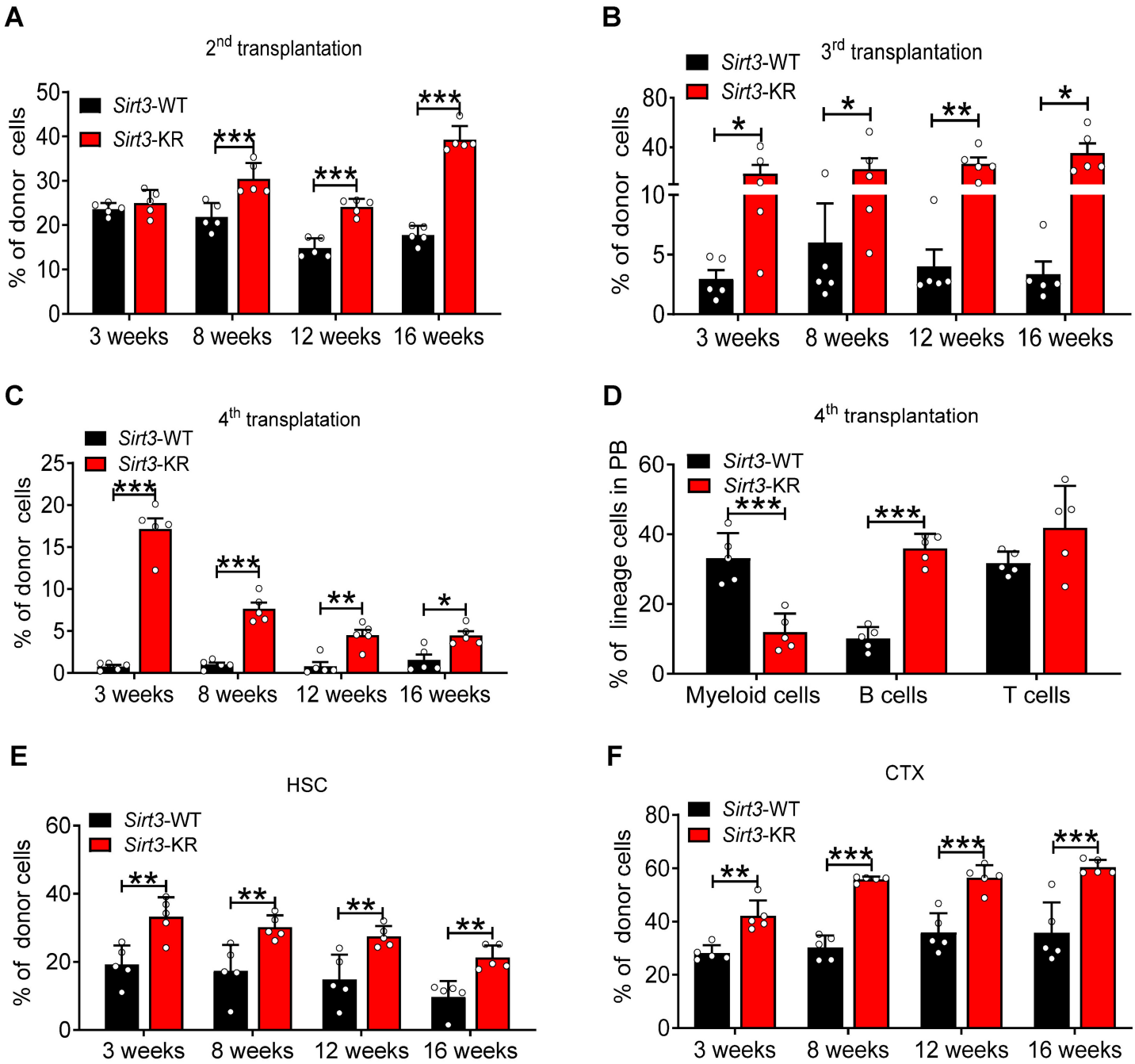
A
2nd transplantation
Sirt3-WT
Sirt3-KR
% of donor cells
3 weeks
8 weeks
12 weeks
16 weeks
B
3rd transplantation
C
4th transplatation
D
4th transplantation
% of lineage cells in PB
Myeloid cells
B cells
T cells
E
HSC
F
CTX

Figure 3

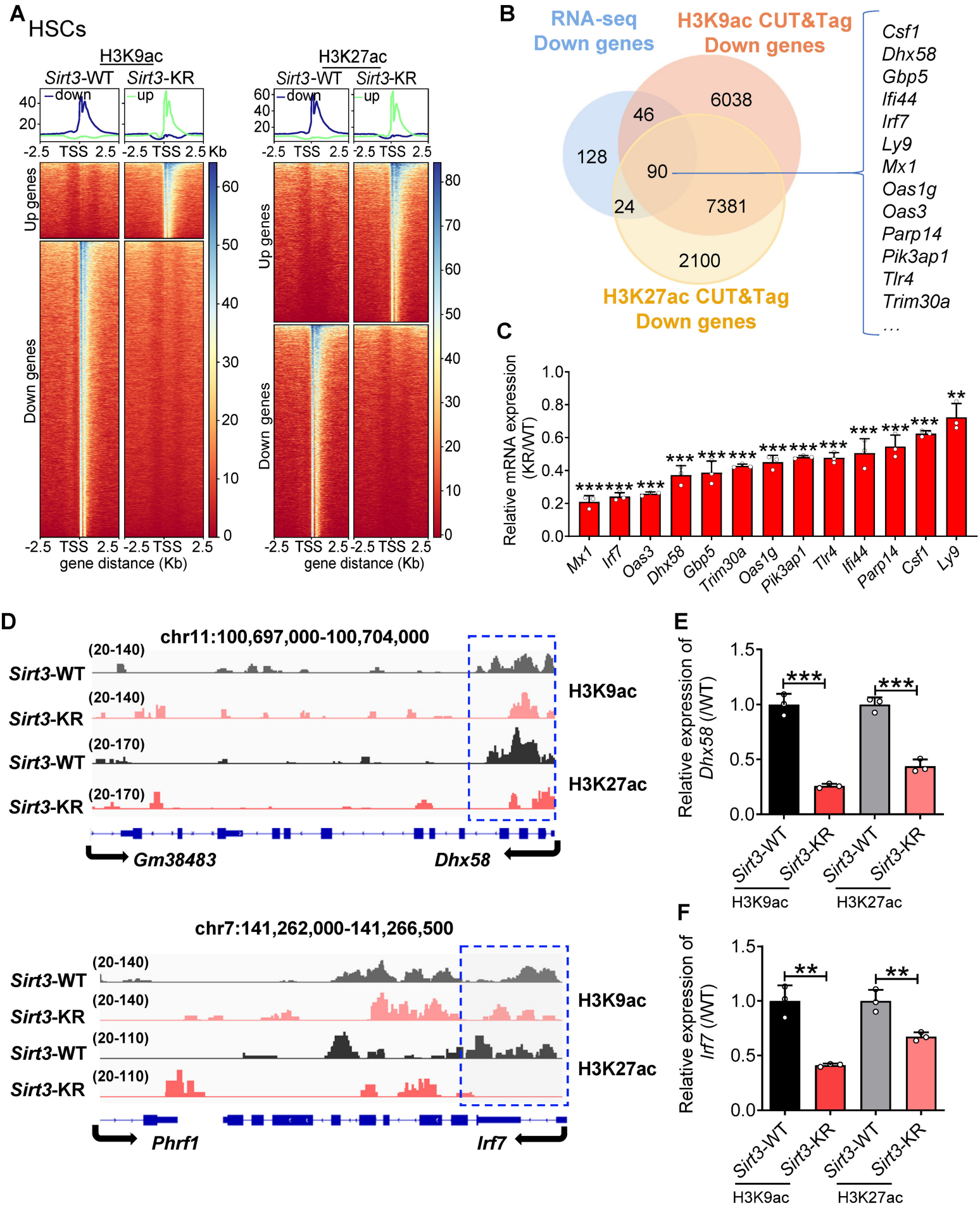
A
HSCs
H3K9ac
H3K27ac
Sirt3-WT
Sirt3-KR
down
up
Up genes
Down genes
-2.5 TSS 2.5 Kb
gene distance (Kb)
B
RNA-seq
Down genes
H3K9ac CUT&Tag
Down genes
H3K27ac CUT&Tag
Down genes
128
46
6038
90
24
7381
2100
Csf1
Dhx58
Gbp5
Ifi44
Irf7
Ly9
Mx1
Oas1g
Oas3
Parp14
Pik3ap1
Tlr4
Trim30a
…
C
Relative mRNA expression (KR/WT)
Mx1
Irf7
Oas3
Dhx58
Gbp5
Trim30a
Oas1g
Pik3ap1
Tlr4
Ifi44
Parp14
Csf1
Ly9
D
chr11:100,697,000-100,704,000
(20-140)
(20-170)
H3K9ac
H3K27ac
Gm38483
Dhx58
chr7:141,262,000-141,266,500
(20-110)
Phrf1
Irf7
E
Relative expression of Dhx58 (/WT)
F
Relative expression of Irf7 (/WT)
H3K9ac
H3K27ac

Figure 4

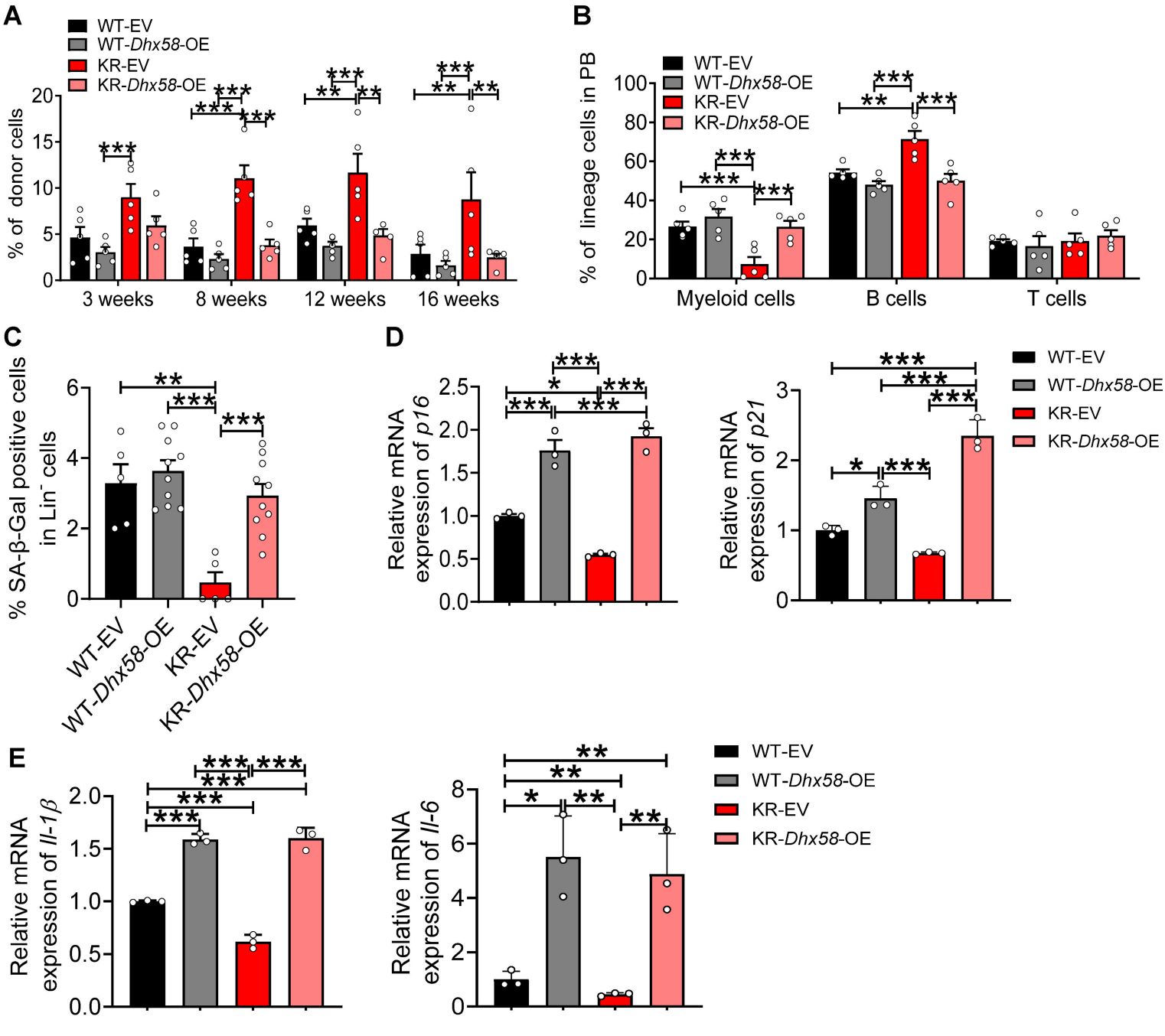
A
WT-EV
WT-Dhx58-OE
KR-EV
KR-Dhx58-OE
% of donor cells
3 weeks
8 weeks
12 weeks
16 weeks
B
% of lineage cells in PB
Myeloid cells
B cells
T cells
C
% SA-β-Gal positive cells in Lin- cells
D
Relative mRNA expression of p16
Relative mRNA expression of p21
E
Relative mRNA expression of Il-1β
Relative mRNA expression of Il-6

Figure 5

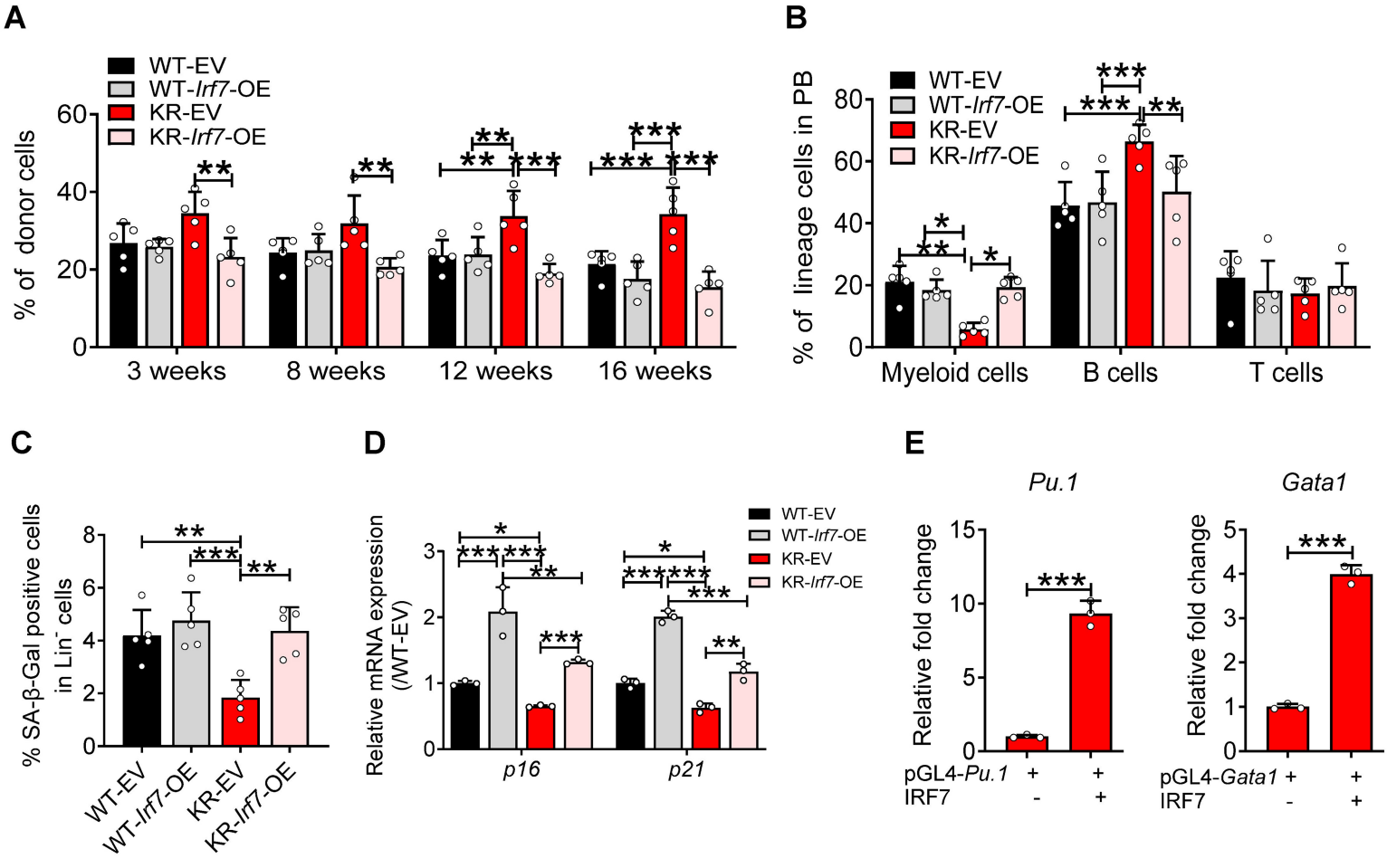
A
WT-EV
WT-Irf7-OE
KR-EV
KR-Irf7-OE
% of donor cells
3 weeks
8 weeks
12 weeks
16 weeks
B
% of lineage cells in PB
Myeloid cells
B cells
T cells
C
% SA-β-Gal positive cells in Lin- cells
D
Relative mRNA expression (/WT-EV)
p16
p21
E
Pu.1
Gata1
Relative fold change
pGL4-Pu.1
pGL4-Gata1
IRF7

Figure 6

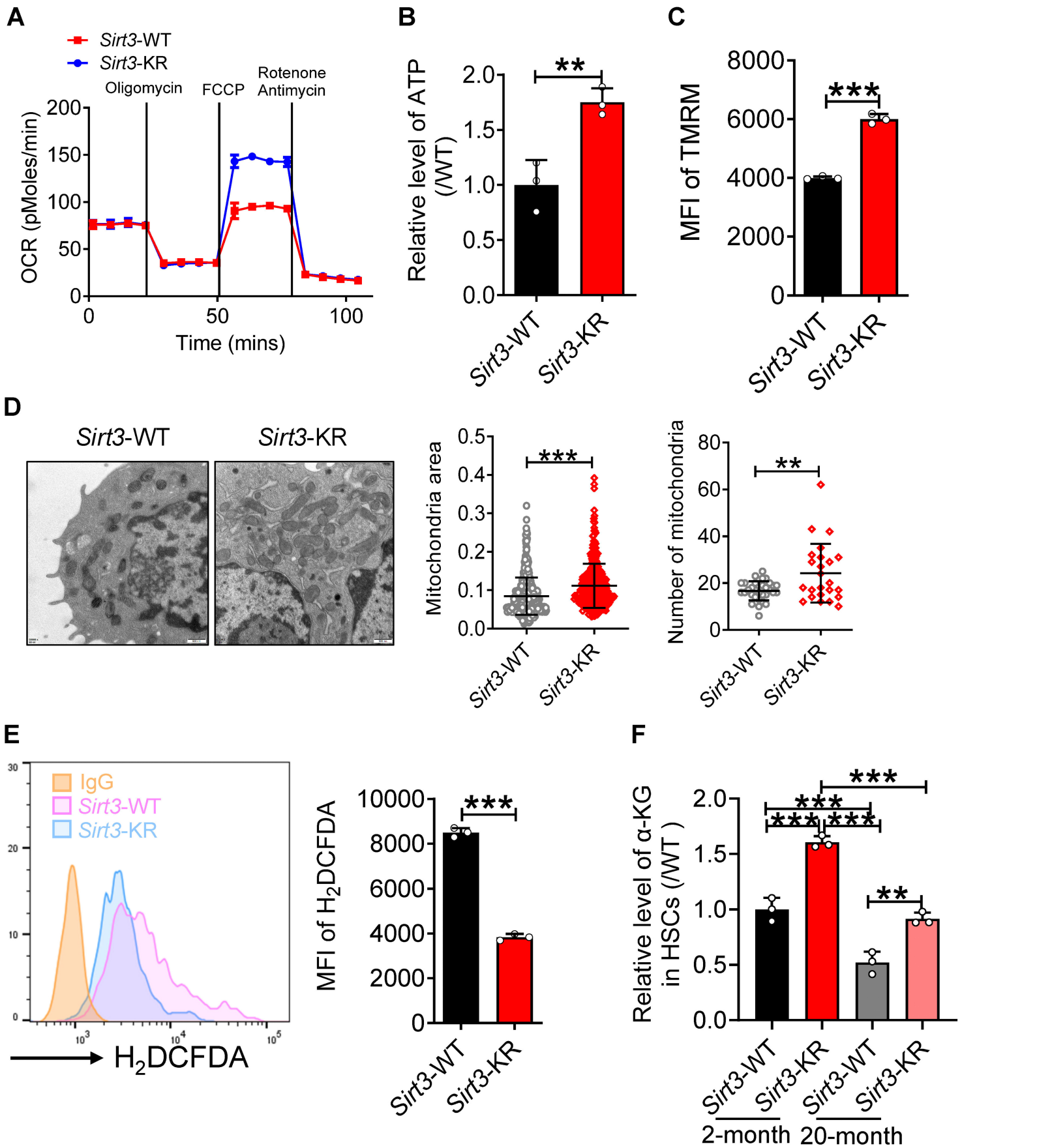
A
Sirt3-WT
Sirt3-KR
Oligomycin
FCCP
Rotenone
Antimycin
OCR (pMoles/min)
Time (mins)
B
Relative level of ATP (/WT)
Sirt3-WT
Sirt3-KR
C
MFI of TMRM
Sirt3-WT
Sirt3-KR
D
Sirt3-WT
Sirt3-KR
Mitochondria area
Number of mitochondria
E
IgG
Sirt3-WT
Sirt3-KR
H2DCFDA
MFI of H2DCFDA
F
Relative level of α-KG in HSCs (/WT)
Sirt3-WT
Sirt3-KR
Sirt3-WT
Sirt3-KR
2-month
20-month

Figure 7

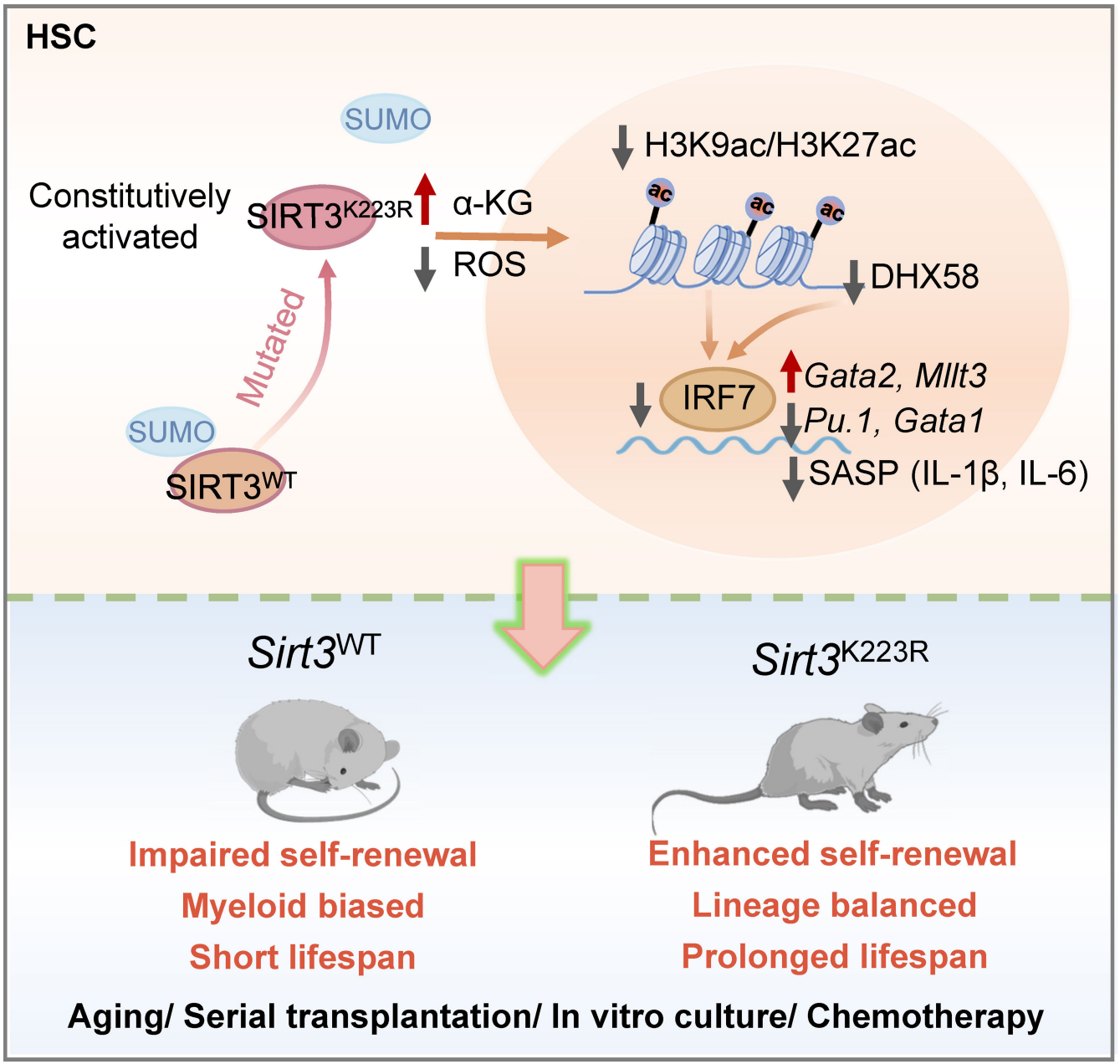
HSC
SUMO
Constitutively activated
SIRT3K223R
α-KG
ROS
Mutated
SUMO
SIRT3WT
H3K9ac/H3K27ac
ac
ac
ac
DHX58
IRF7
Gata2, Mllt3
Pu.1, Gata1
SASP (IL-1β, IL-6)
Sirt3WT
Sirt3K223R
Impaired self-renewal
Myeloid biased
Short lifespan
Enhanced self-renewal
Lineage balanced
Prolonged lifespan
Aging/ Serial transplantation/ In vitro culture/ Chemotherapy

Figure S1

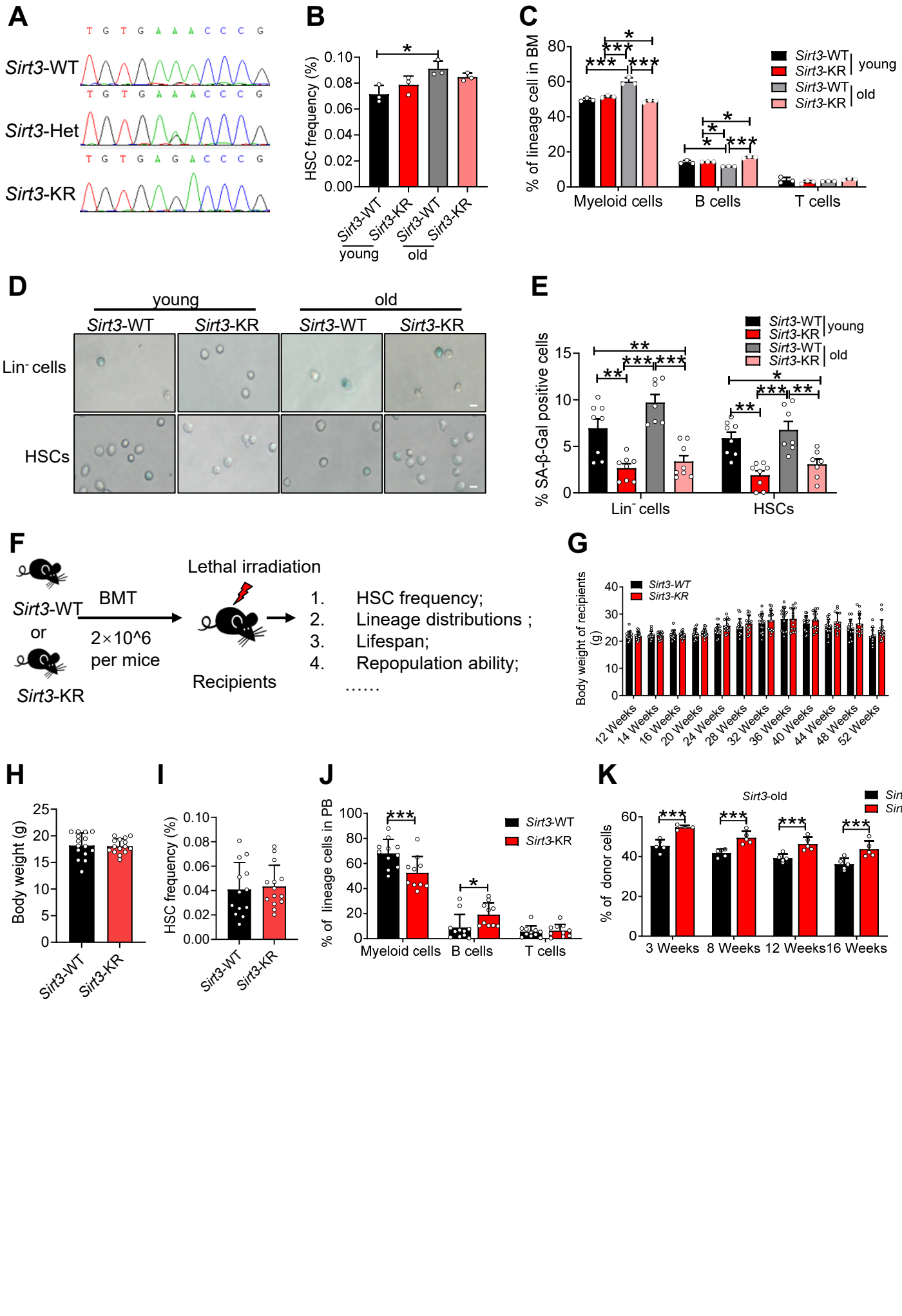
A
Sirt3-WT
Sirt3-Het
Sirt3-KR
B
HSC frequency (%)
Sirt3-WT
Sirt3-KR
young
old
C
% of lineage cell in BM
Myeloid cells
B cells
T cells
young
old
D
young
old
Lin- cells
HSCs
E
% SA-β-Gal positive cells
Lin- cells
HSCs
F
Sirt3-WT
or
Sirt3-KR
BMT
2×10^6
per mice
Lethal irradiation
Recipients
1. HSC frequency;
2. Lineage distributions ;
3. Lifespan;
4. Repopulation ability;
……
G
Body weight of recipients (g)
H
Body weight (g)
I
HSC frequency (%)
J
% of lineage cells in PB
Myeloid cells
B cells
T cells
K
Sirt3-old
% of donor cells
3 Weeks
8 Weeks
12 Weeks
16 Weeks

Figure S1. Related to Figure 1. SIRT3 activation inhibits HSC aging under stress conditions and markedly extends the overall lifespan of mice. A) Schematic diagram of the construction of the SIRT3 SUMOylation site mutant mouse strains. B) The frequencies of immunophenotypic $Lin^{-}Sca\text{-}1^{+}c\text{-}Kit^{+}CD34^{-}CD135^{-}$ LT-HSCs in the BM of young or old *Sirt3*-WT and *Sirt3*-KR mice were quantitated by flow cytometric analysis. C) The frequencies of myeloid cells ($Mac\text{-}1^{+}$ and $Gr\text{-}1^{+}$), B cells ($B220^{+}$) and T cells ($CD3e^{+}$) in the BM of young or old *Sirt3*-WT and *Sirt3*-KR mice were quantitated by flow cytometric analysis. D) SA-β-Gal staining of BM cells from young or old *Sirt3*-WT and *Sirt3*-KR mice are shown. Scale bar, 10 μm. E) Frequencies of SA-β-Gal cells among Lin^{-} and HSCs in the BM of young or old *Sirt3*-WT and *Sirt3*-KR mice. F) Schematic diagram of the strategy used to construct the aging model. G) Body weight of the recipient mice receiving *Sirt3*-WT or *Sirt3*-KR BM donor cells was monitored from 12 to 52 weeks. H) Body weight of recipient mice at the end stage was monitored. I) HSC frequency in recipient mice at end stage. J) Percentages of myeloid, B, and T cells in PB of recipient mice at end stage. K) The repopulation ability of donor cells from aged (24-month-old) *Sirt3*-WT and *Sirt3*-KR mice was determined by flow cytometric analysis at the indicated time points (n=5). (Each dot represents an individual mouse). *P<0.05, **P<0.01, ***P<0.001.

Figure S2

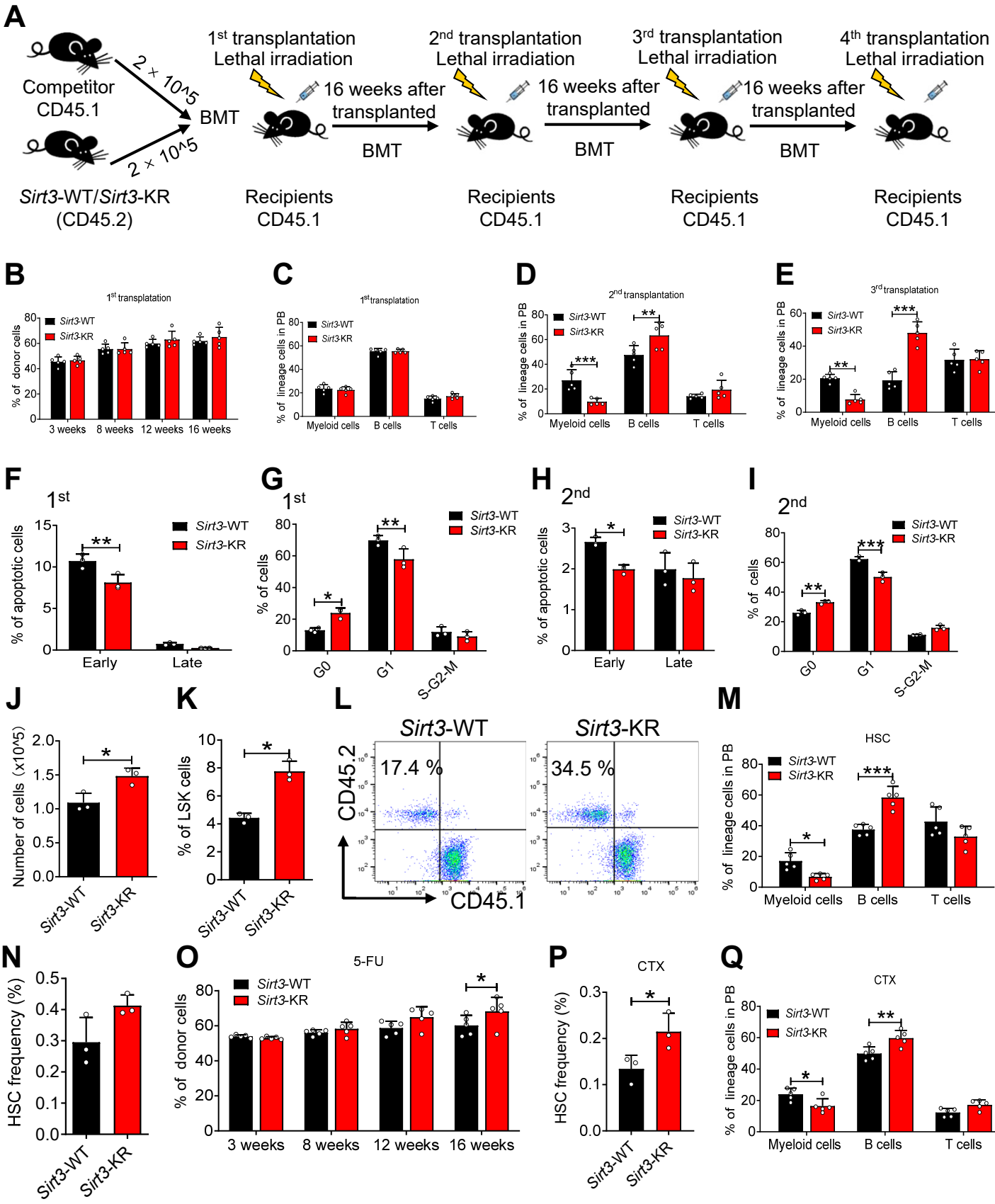
A
Competitor CD45.1
2 × 10^5
BMT
2 × 10^5
Sirt3-WT/Sirt3-KR (CD45.2)
1st transplantation Lethal irradiation
16 weeks after transplanted
BMT
Recipients CD45.1
2nd transplantation Lethal irradiation
16 weeks after transplanted
BMT
Recipients CD45.1
3rd transplantation Lethal irradiation
16 weeks after transplanted
BMT
Recipients CD45.1
4th transplantation Lethal irradiation
Recipients CD45.1
B
1st transplatation
% of donor cells
Sirt3-WT
Sirt3-KR
3 weeks
8 weeks
12 weeks
16 weeks
C
1st transplatation
% of lineage cells in PB
Myeloid cells
B cells
T cells
D
2nd transplantation
E
3rd transplatation
F
1st
% of apoptotic cells
Early
Late
G
1st
% of cells
G0
G1
S-G2-M
H
2nd
I
2nd
J
Number of cells (x10^5)
K
% of LSK cells
L
Sirt3-WT
Sirt3-KR
17.4 %
34.5 %
CD45.2
CD45.1
M
HSC
N
HSC frequency (%)
O
5-FU
P
CTX
Q
CTX

Figure S2. Related to Figure 2. The deSUMOylation of SIRT3 preserves HSC self-renewal under stress conditions. A) Schematic diagram of the strategy for serial bone marrow transplantation. B) Repopulation of *Sirt3*-WT and *Sirt3*-KR donor cells was measured 3 to 16 weeks after the 1st transplantation (n=5). C-E) Multilineage differentiation of donor cells into myeloid cells (Mac-1^{+} Gr-1^{+}), B cells (B220^{+}), and T cells (CD3^{+}) in PB was quantitated by flow cytometry at 16 weeks after the 1st (C), 2nd (D) and 3rd (E) transplantations (n=5). F-G) Frequencies of apoptotic LT-HSCs (F) and the cell cycle status of HSCs (G) derived from *Sirt3*-WT and *Sirt3*-KR donor cells were measured after the 1^{s} transplantation (n=3). H-I) Frequencies of apoptotic LT-HSCs (H) and the cell cycle status of HSCs (I) derived from *Sirt3*-WT and *Sirt3*-KR donor cells were measured after the secondary transplantation (n=3). J) Total cell numbers of cultured *Sirt3*-WT and *Sirt3*-KR HSCs after 8 days of *in vitro* culture. K) HSCs from *Sirt3*-WT and *Sirt3*-KR mice were cultured for 8 days, and the frequencies of Lin^{-}Sca-1^{+}c-Kit^{+} (LSK) cells were assessed by flow cytometric analysis (n=3). L) Representative flow cytometric analyses of the repopulation of cultured HSCs from *Sirt3*-WT and *Sirt3*-KR mice at 8 weeks post-transplantation. M) Multilineage contribution of donor cells in PB was quantified at 16 weeks after transplantation (n=5). N) Frequencies of immunophenotypic Lin^{-}Sca-1^{+}c-Kit^{+}CD34^{-}CD135^{-} LT-HSCs in the BM of *Sirt3*-WT and *Sirt3*-KR mice after 5-FU treatment (n=3). O) The repopulation of *Sirt3*-WT and *Sirt3*-KR donor cells after 5-FU treatment was measured by flow cytometry at the indicated time points after transplantation (n=5). P) Frequencies of immunophenotypic Lin^{-}Sca-1^{+}c-Kit^{+}CD34^{-}CD135^{-} LT-HSCs in the BM of *Sirt3*-WT and *Sirt3*-KR mice after cyclophosphamide (CTX) treatment (n=3). Q) The multilineage contribution of donor cells in PB was quantified at 16 weeks after CTX treatment and transplantation (n=5). *P<0.05, **P<0.01, ***P<0.001.

Figure S3

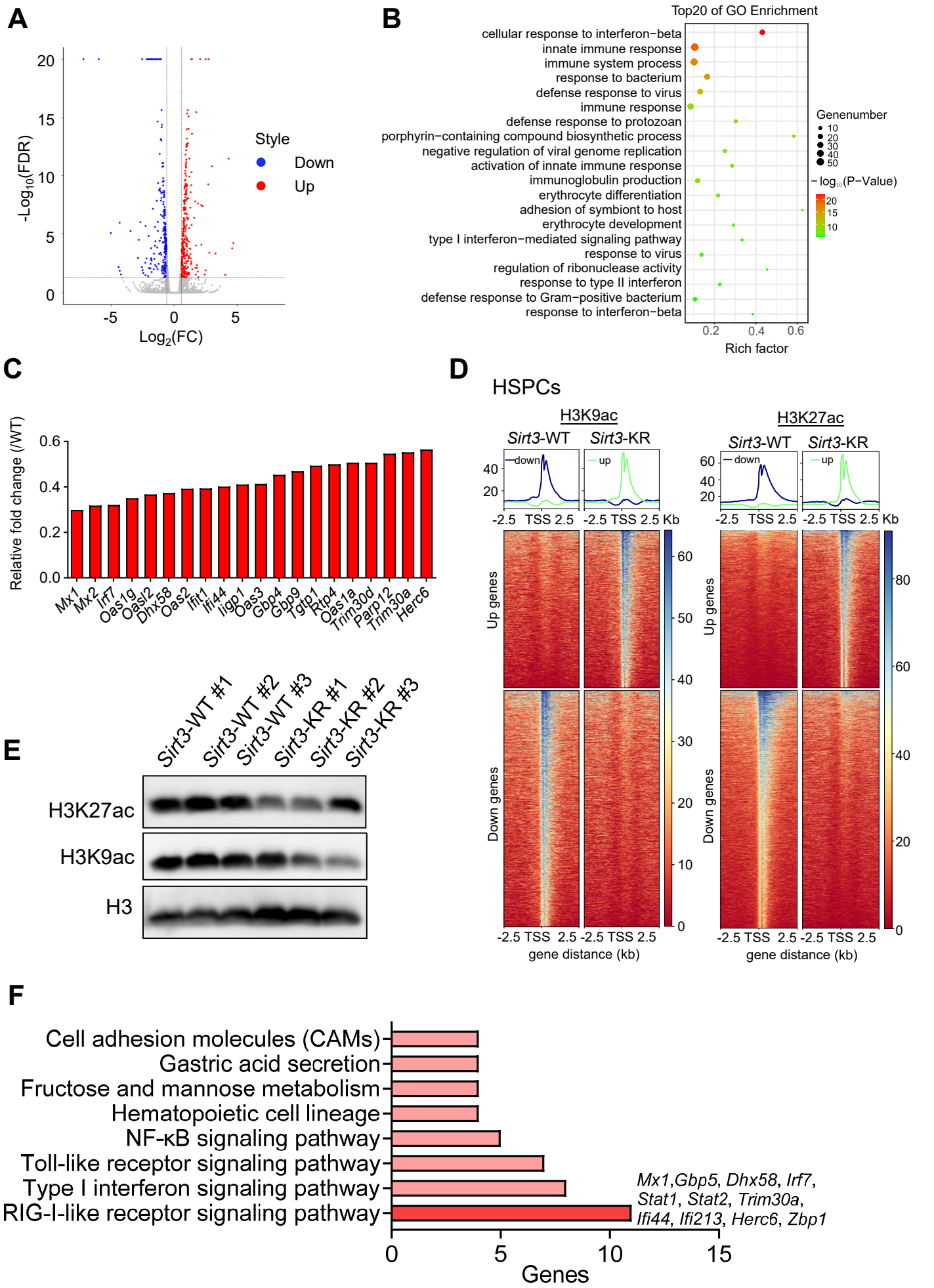
A
-Log10(FDR)
Log2(FC)
Style
Down
Up
B
Top20 of GO Enrichment
cellular response to interferon−beta
innate immune response
immune system process
response to bacterium
defense response to virus
immune response
defense response to protozoan
porphyrin−containing compound biosynthetic process
negative regulation of viral genome replication
activation of innate immune response
immunoglobulin production
erythrocyte differentiation
adhesion of symbiont to host
erythrocyte development
type I interferon−mediated signaling pathway
response to virus
regulation of ribonuclease activity
response to type II interferon
defense response to Gram−positive bacterium
response to interferon−beta
Rich factor
Genenumber
− log10(P−Value)
C
Relative fold change (/WT)
Mx1
Mx2
Irf7
Oas1g
Oasl2
Dhx58
Oas2
Ifit1
Ifi44
Iigp1
Oas3
Gbp4
Gbp9
Tgtp1
Rtp4
Oas1a
Trim30d
Parp12
Trim30a
Herc6
D
HSPCs
H3K9ac
H3K27ac
Sirt3-WT
Sirt3-KR
down
up
Up genes
Down genes
gene distance (kb)
E
Sirt3-WT #1
Sirt3-WT #2
Sirt3-WT #3
Sirt3-KR #1
Sirt3-KR #2
Sirt3-KR #3
H3K27ac
H3K9ac
H3
F
Cell adhesion molecules (CAMs)
Gastric acid secretion
Fructose and mannose metabolism
Hematopoietic cell lineage
NF-κB signaling pathway
Toll-like receptor signaling pathway
Type I interferon signaling pathway
RIG-I-like receptor signaling pathway
Mx1,Gbp5, Dhx58, Irf7,
Stat1, Stat2, Trim30a,
Ifi44, Ifi213, Herc6, Zbp1
Genes

Figure S3. Related to Figure 3. SIRT3 negatively regulates target genes in the RIG-1 signaling pathway by deacetylating H3K9ac and H3K27ac in HSCs. A) Volcano plots showing differentially expressed genes in *Sirt3*-WT and *Sirt3*-KR HSCs. A total of 305 genes were significantly upregulated, whereas 288 genes were downregulated in *Sirt3*-KR HSCs. B) Changes in pathways in HSCs from *Sirt3*-WT and *Sirt3*-KR mice evaluated by RNA-sequencing (RNA-seq) analyses. C) The downregulated expression of potential candidate genes related to signaling pathways involved in the inflammatory response in *Sirt3*-KR HSCs (compared with *Sirt3*-WT HSCs) were analyzed by RNA-seq. D) Heatmap showing CUT&Tag-seq coverage at sites with altered H3K9ac and H3K27ac modifications in *Sirt3*-WT and *Sirt3*-KR hematopoietic stem/progenitor cells (HSPCs). E) The levels of H3K9ac and H3K27ac in *Sirt3*-WT and *Sirt3*-KR HSPCs were determined by western blotting. F) KEGG enrichment analysis of the 90 commonly downregulated genes in *Sirt3*-KR HSCs identified by RNA-seq and H3K9ac/H3K27ac CUT&Tag, showing the top 8 enriched pathways. The x-axis represents the number of genes enriched in each pathway.

Figure S4

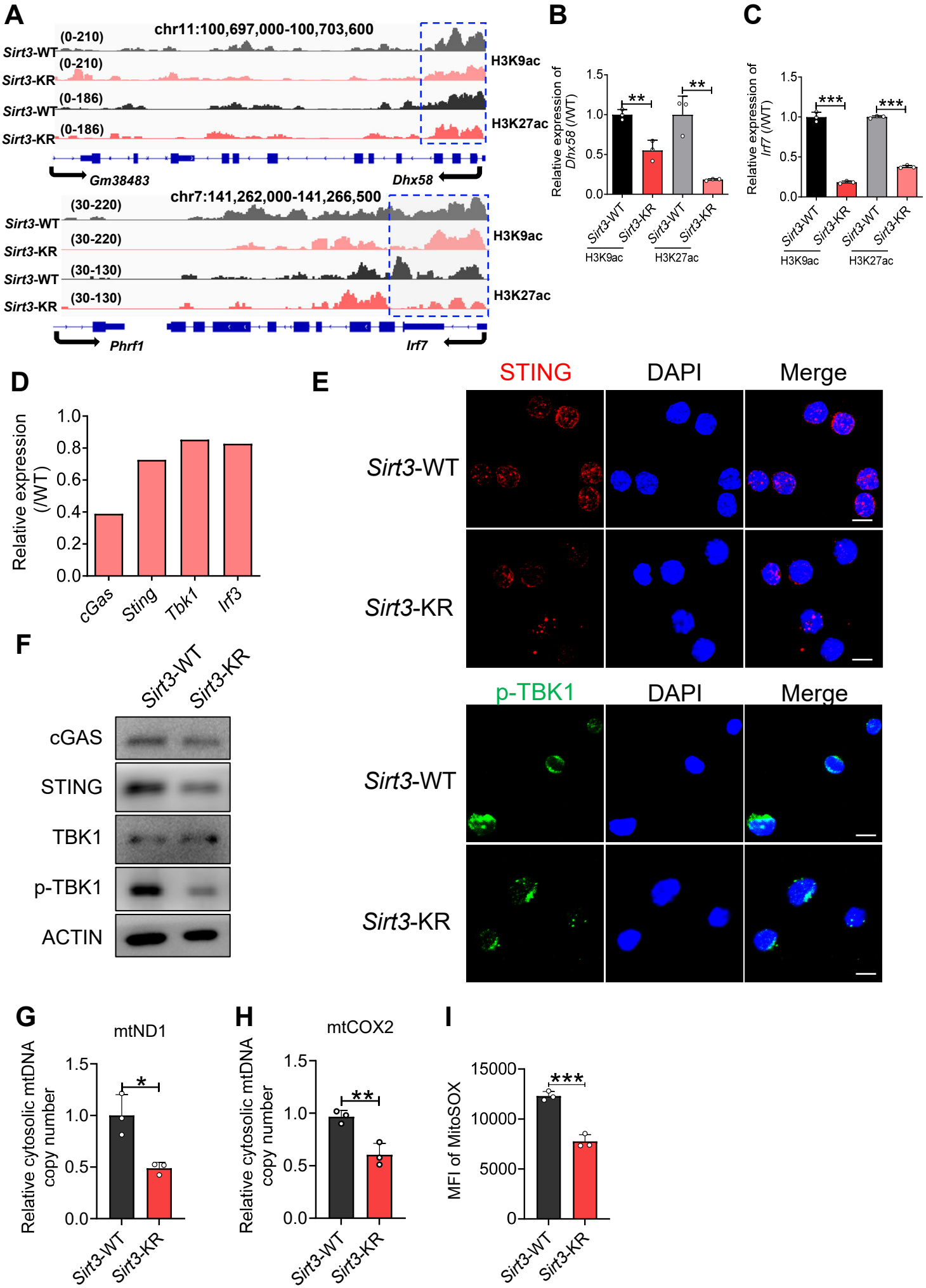
A
chr11:100,697,000-100,703,600
(0-210)
Sirt3-WT
(0-210)
Sirt3-KR
(0-186)
Sirt3-WT
(0-186)
Sirt3-KR
H3K9ac
H3K27ac
Gm38483
Dhx58
chr7:141,262,000-141,266,500
(30-220)
Sirt3-WT
(30-220)
Sirt3-KR
(30-130)
Sirt3-WT
(30-130)
Sirt3-KR
H3K9ac
H3K27ac
Phrf1
Irf7
B
Relative expression of Dhx58 (/WT)
Sirt3-WT
Sirt3-KR
Sirt3-WT
Sirt3-KR
H3K9ac
H3K27ac
C
Relative expression of Irf7 (/WT)
Sirt3-WT
Sirt3-KR
Sirt3-WT
Sirt3-KR
H3K9ac
H3K27ac
D
Relative expression (/WT)
cGas
Sting
Tbk1
Irf3
E
STING
DAPI
Merge
Sirt3-WT
Sirt3-KR
p-TBK1
DAPI
Merge
Sirt3-WT
Sirt3-KR
F
Sirt3-WT
Sirt3-KR
cGAS
STING
TBK1
p-TBK1
ACTIN
G
mtND1
Relative cytosolic mtDNA copy number
Sirt3-WT
Sirt3-KR
H
mtCOX2
Relative cytosolic mtDNA copy number
Sirt3-WT
Sirt3-KR
I
MFI of MitoSOX
Sirt3-WT
Sirt3-KR

Figure S4. Related to Figure 3. SIRT3 sustains HSC activities and delays aging by regulating inflammation-associated pathways. A) Analysis of H3K9ac and H3K27ac CUT&Tag-seq at peaks in the genomic regions of DHX58 and IRF7. B) ChIP-qPCR analysis of the H3K9ac and H3K27ac levels at the *Dhx58* promoter in *Sirt3*-WT and *Sirt3*-KR HSPCs. C) ChIP-qPCR analysis of the H3K9ac and H3K27ac levels at the *Irf7* promoter in *Sirt3*-WT and *Sirt3*-KR HSPCs. D) The relative expression levels of candidate genes related to the cGAS-STING signaling pathway in *Sirt3*-KR HSCs are shown (compared to that of *Sirt3*-WT HSCs). E) Immunofluorescence staining showing STING and p-TBK1 levels in *Sirt3*-WT and *Sirt3*-KR HSCs. Scale bar, 10 μm. F) The levels of cGAS, STING, TBK1 and p-TBK1 in *Sirt3*-WT and *Sirt3*-KR HSCs were determined by western blotting. G-H) Relative copy number of cytosolic mtDNA (*mtND1*, G; *mtCOX2*, H) in *Sirt3*-WT and *Sirt3*-KR HSPCs. I) Mean fluorescence intensity (MFI) of MitoSOX in *Sirt3*-WT and *Sirt3*-KR HSCs. *P<0.05, **P<0.01, ***P<0.001.

Figure S5

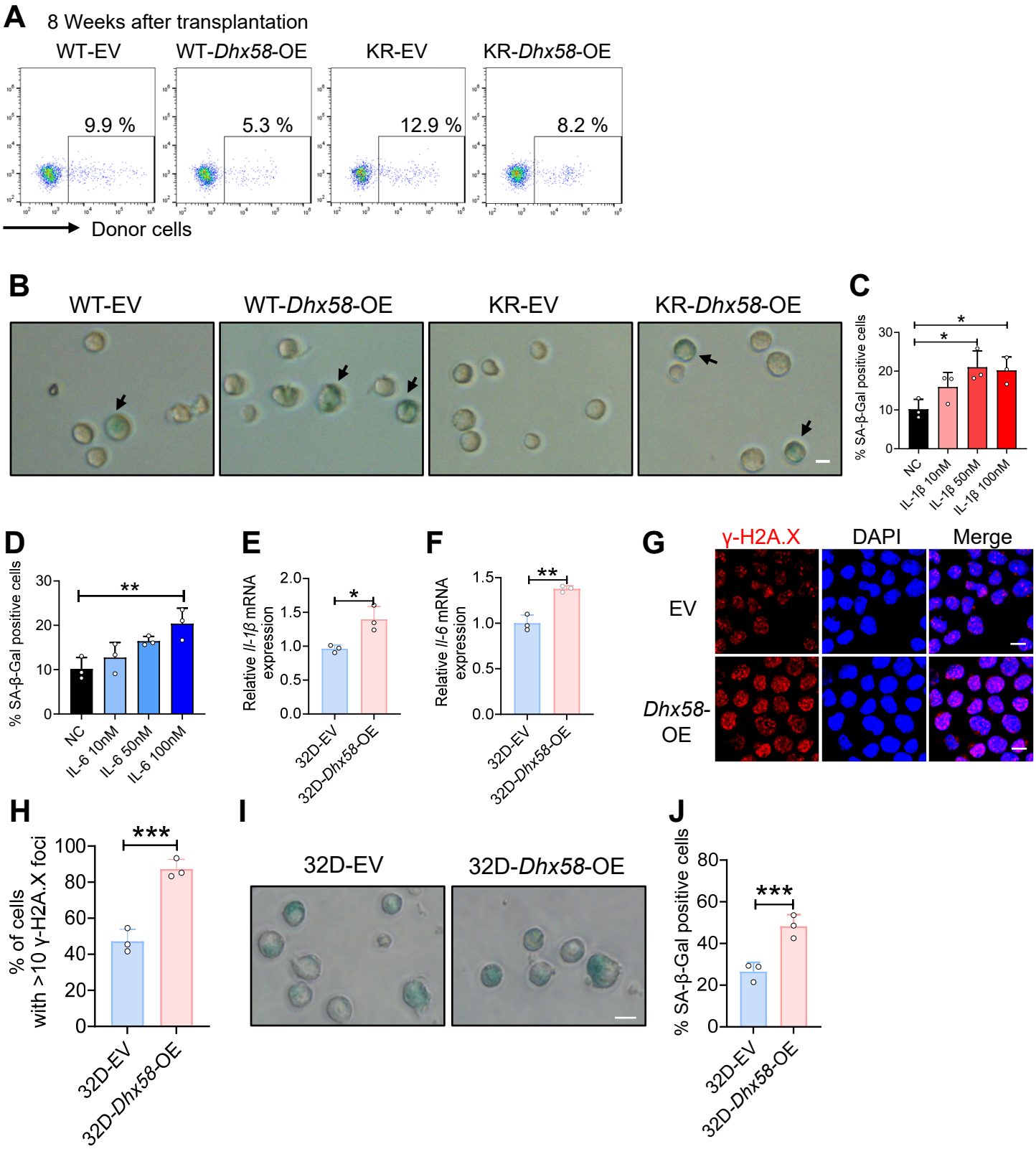
A
8 Weeks after transplantation
WT-EV
WT-Dhx58-OE
KR-EV
KR-Dhx58-OE
9.9 %
5.3 %
12.9 %
8.2 %
Donor cells
B
WT-EV
WT-Dhx58-OE
KR-EV
KR-Dhx58-OE
C
% SA-β-Gal positive cells
NC
IL-1β 10nM
IL-1β 50nM
IL-1β 100nM
D
% SA-β-Gal positive cells
NC
IL-6 10nM
IL-6 50nM
IL-6 100nM
E
Relative Il-1β mRNA expression
32D-EV
32D-Dhx58-OE
F
Relative Il-6 mRNA expression
32D-EV
32D-Dhx58-OE
G
γ-H2A.X
DAPI
Merge
EV
Dhx58-OE
H
% of cells with >10 γ-H2A.X foci
32D-EV
32D-Dhx58-OE
I
32D-EV
32D-Dhx58-OE
J
% SA-β-Gal positive cells
32D-EV
32D-Dhx58-OE

Figure S5. Related to Figure 4. SIRT3 promotes HSC self-renewal and delays HSC aging through the downregulation of DHX58. A) Representative flow cytometric analyses of the repopulation of HSCs from *Sirt3*-WT and *Sirt3*-KR mice with/without *Dhx58* overexpression (RFP^+ cells) at 8 weeks post-transplantation. B) Representative images of SA-β-Gal-stained BM cells from *Sirt3*-WT, *Sirt3*-KR, *Dhx58*-overexpressing *Sirt3*-WT or *Sirt3*-KR. Scale bar, 10 μm. C-D) Percentages of SA-β-Gal-positive 32D cells after treatment with different doses of IL-1β (C) or IL-6 (D) for 7 days (n=3). E-F) The relative mRNA levels of *Il-1β* (E) and *Il-6* (F) in 32D cells with/without overexpression of *Dhx58* were measured by qRT-PCR (n=3). G) Immunofluorescence staining showing γ-H_2A.X levels in 32D cells with/without overexpression of *Dhx58*. Scale bar, 10 μm. H) The proportions of cells with more than 10 γ-H2A.X foci in G were calculated (n=3). I) Representative SA-β-Gal staining of 32D cells with/without overexpression of *Dhx58* is shown. Scale bar, 10 μm. J) The percentage of SA-β-Gal-positive 32D cells with/without overexpression of *Dhx58* (n=3). *P<0.05, **P<0.01, ***P<0.001.

Figure S6

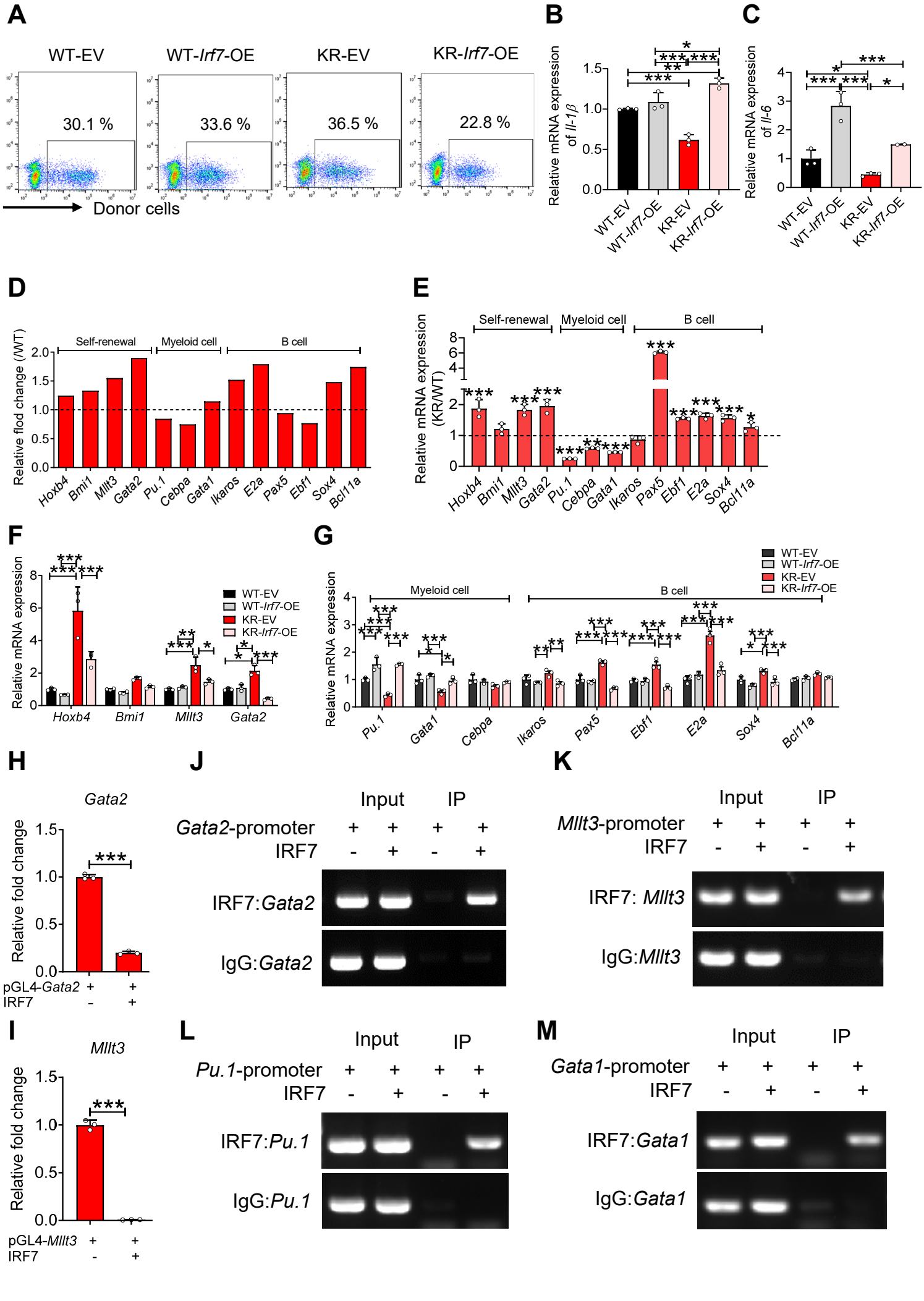
A
WT-EV
WT-Irf7-OE
KR-EV
KR-Irf7-OE
30.1 %
33.6 %
36.5 %
22.8 %
Donor cells
B
Relative mRNA expression of Il-1β
C
Relative mRNA expression of Il-6
D
Relative flod change (/WT)
Self-renewal
Myeloid cell
B cell
Hoxb4
Bmi1
Mllt3
Gata2
Pu.1
Cebpa
Gata1
Ikaros
E2a
Pax5
Ebf1
Sox4
Bcl11a
E
Relative mRNA expression (KR/WT)
F
Relative mRNA expression
WT-EV
WT-Irf7-OE
KR-EV
KR-Irf7-OE
G
H
Gata2
Relative fold change
pGL4-Gata2
IRF7
J
Input
IP
Gata2-promoter
IRF7
IRF7:Gata2
IgG:Gata2
K
Mllt3-promoter
IRF7: Mllt3
IgG:Mllt3
I
Mllt3
pGL4-Mllt3
L
Pu.1-promoter
IRF7:Pu.1
IgG:Pu.1
M
Gata1-promoter
IRF7:Gata1
IgG:Gata1

Figure S6. Related to Figure 5. IRF7 serves as a DHX58 downstream target to regulate HSC stemness and aging. A) Representative flow cytometric analyses of the repopulation of HSCs from *Sirt3*-WT and *Sirt3*-KR mice with/without *Irf7* overexpression (RFP^+ cells). B-C) The relative mRNA levels of the senescence-associated secretory phenotypes (SASP) genes *Il-1β* (B) and *Il-6* (C) were measured in *Sirt3*-WT, *Sirt3*-KR, *Irf7*-overexpressing *Sirt3*-WT or *Sirt3*-KR HSCs by qRT-PCR (n=3). D) The relative expression levels of candidate genes related to self-renewal and lineage differentiation in *Sirt3*-KR HSCs (compared with *Sirt3*-WT HSCs) were analyzed by RNA-seq. E) The relative mRNA expression levels of self-renewal-related and lineage differentiation-related genes in *Sirt3*-KR HSCs (compared with *Sirt3*-WT HSCs) were determined by qRT-PCR (n=3). F) The relative mRNA expression of self-renewal-related candidate genes in *Sirt3*-WT, *Sirt3*-KR, and *Irf7*-overexpressing *Sirt3*-WT or *Sirt3*-KR HSCs determined by qRT-PCR (n=3). G) The relative mRNA expression of lineage differentiation-related candidate genes in *Sirt3*-WT, *Sirt3*-KR, *Irf7*-overexpressing *Sirt3*-WT or *Sirt3*-KR HSCs determined by qRT-PCR (n=3). H-I) A luciferase reporter assay was performed to evaluate the transcriptional activity of IRF7 at the promoters of *Gata2* (H) and *Mllt3* (I) (n=3). J-M) The binding of IRF7 to the *Gata2* (J), *Mllt3* (K), *Pu.1* (L) and *Gata1* (M) promoter regions was determined by a ChIP assay. *P<0.05, **P<0.01, ***P<0.001.

Figure S7

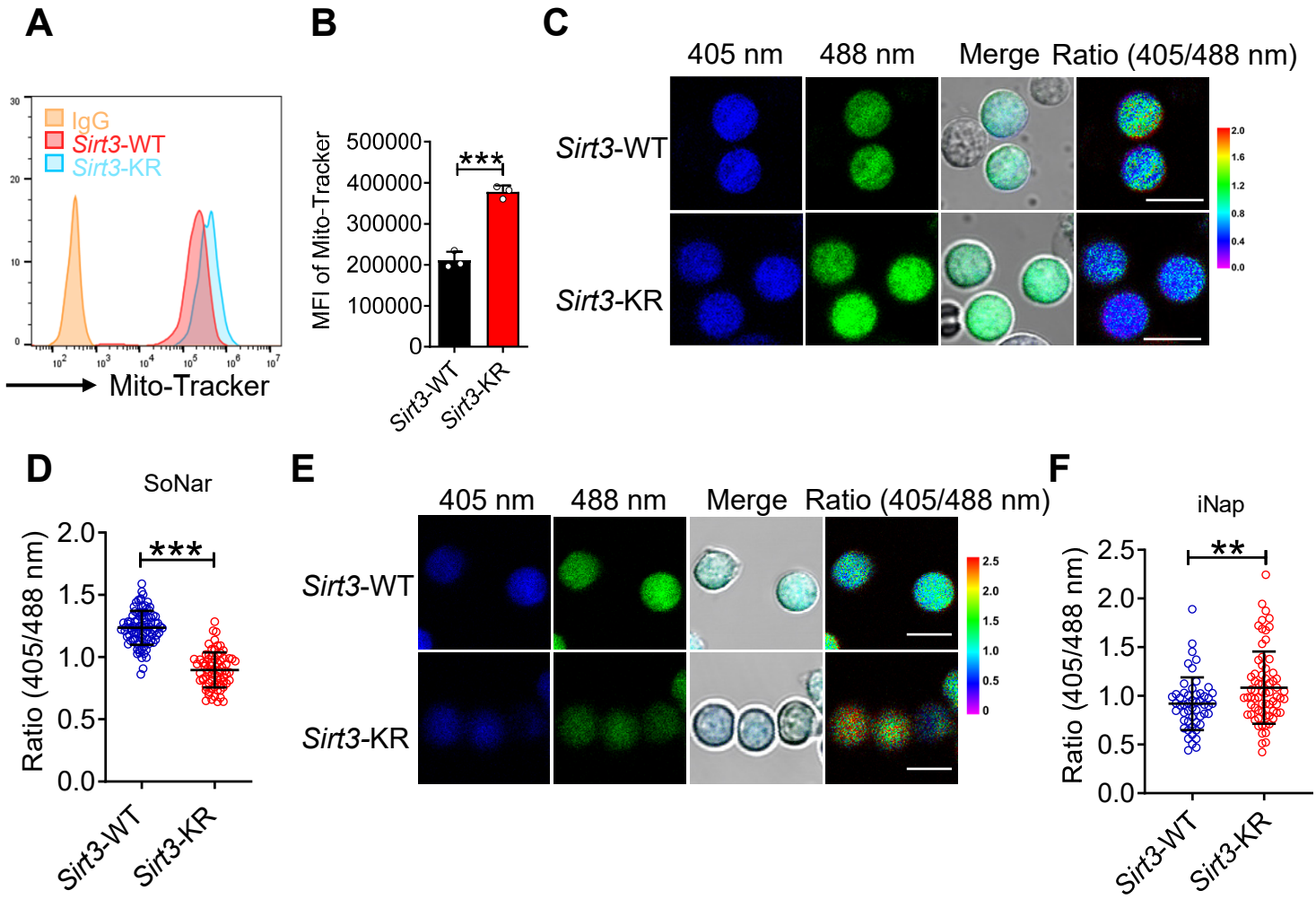
A
IgG
Sirt3-WT
Sirt3-KR
Mito-Tracker
B
MFI of Mito-Tracker
***
Sirt3-WT
Sirt3-KR
C
405 nm
488 nm
Merge
Ratio (405/488 nm)
Sirt3-WT
Sirt3-KR
D
SoNar
Ratio (405/488 nm)
***
Sirt3-WT
Sirt3-KR
E
405 nm
488 nm
Merge
Ratio (405/488 nm)
Sirt3-WT
Sirt3-KR
F
iNap
Ratio (405/488 nm)
**
Sirt3-WT
Sirt3-KR
G
Anti-Oxidative related genes
Glycolysis
Oxidative phosphorylation
PPP
Relative mRNA expression (/WT)
Sod1
Sod2
Txn1
Prdx1
Prdx2
Prdx3
Prdx4
Prdx5
Prdx6
Gpx1
Gpx2
Gpx3
Txnrd1
Txnrd2
Txnrd3
Txndc17
Glrx1
Glrx2
Glrx3
Nox1
Nox2
Gsr
Glut2
Glut3
Glut4
Hk1
Pfkl
Pfkm
Gapdh
Pkm2
Ldha
Mdh1
Mdh2
Idh1
Idh2
Idh3a
Idh3b
Idh3g
Aco2
Atp5i
Atp5o
Cox6b1
Cox18
Ndufb5
G6pd
Pgd

Figure S7. Related to Figure 6. SIRT3 enhances mitochondrial metabolism and α-KG generation in HSCs. A) Representative flow cytometric analyses of Mito-Tracker staining in *Sirt3*-WT and *Sirt3*-KR HSCs. B) Quantification data of the Mito-Tracker MFI in *Sirt3*-WT and *Sirt3*-KR HSCs at panel A (n=3). C) Representative images of the fluorescence ratios (F_{405}/F_{488} nm) in the HSCs derived from *Sirt3*-WT-SoNar and *Sirt3*-KR-SoNar mice. Scale bar, 10 μm. D) Quantification of the SoNar fluorescence ratio (F_{405}/F_{488} nm) in the HSCs of *Sirt3*-WT-SoNar and *Sirt3*-KR-SoNar mice in panel C (WT: n=98; KR: n=76). E) Representative images of the fluorescence ratio (F_{405}/F_{488} nm) in the HSCs of *Sirt3*-WT-iNap and *Sirt3*-KR-iNap mice. Scale bar, 10 μm. F) Quantification of the iNap fluorescence ratio (F_{405}/F_{488} nm) in the HSCs of *Sirt3*-WT-iNap and *Sirt3*-KR-iNap mice in panel E (WT: n=53; KR: n=70). G) The relative mRNA expression levels of redox homeostasis-related, glycolysis and oxidative phosphorylation related candidate genes in *Sirt3*-WT and *Sirt3*-KR HSCs were determined by qRT-PCR (n=3). *P<0.05, **P<0.01, ***P<0.001.

Supplemental Methods and Materials

Animals

Sirt3-K223R mutant mice (*Sirt3*-KR) were obtained from Dr. Jinke Cheng's Laboratory (Shanghai Jiao Tong University, China). CD45.1 mice were provided by Dr. Jiang Zhu at Ruijin Hospital, Shanghai, China. For all experiments, 6- to 8-week-old C57BL/6 CD45.2 mice were ordered from the Shanghai SLAC Laboratory Animal Company (Shanghai, China) and maintained at the Animal Core Facility at Shanghai Jiao Tong University School of Medicine.

Competitive reconstitution analysis

For the analysis of the function of SIRT3 in HSC activities, a serial competitive reconstitution analysis was performed with *Sirt3*-WT or *Sirt3*-KR mice, and a total of 2×10^5 *Sirt3*-WT or *Sirt3*-KR CD45.2 donor bone marrow (BM) cells were mixed with 2×10^5 CD45.1 competitor BM cells and transplanted into lethally irradiated CD45.1 recipient mice by retroorbital injection.

In other stress conditions, $Lin^-Sca1^+c\text{-}Kit^+CD34^-CD135^-$ LT-HSCs were sorted from *Sirt3*-WT and *Sirt3*-KR mice, cultured for 8 days *in vitro*, and then injected into lethally irradiated recipient mice along with 2×10^5 CD45.1 competitor cells. In some cases, six-week-old *Sirt3*-WT and *Sirt3*-KR mice were treated with 200 mg/kg cyclophosphamide (CTX) for 4 weeks or with 150 mg/kg 5-fluorouracil (5-FU) for 6 days through intraperitoneal injection. Then, 2×10^5 *Sirt3*-WT or *Sirt3*-KR BM cells together with 3×10^5 CD45.1 competitors were transplanted into lethally irradiated CD45.1 mice.

For the rescue experiments, the retroviral XZ201-*Dhx58*-HA-mCherry-expressing plasmid, XZ201-*Irf7*-HA-mCherry or empty vector was mixed with the pCL-ECO

packaging plasmid at a ratio of 2:1 and transfected into 293T cells. The virus-containing supernatant was harvested for the infection of lineage-negative (Lin^{-}) cells isolated from *Sirt3*-WT or *Sirt3*-KR mice, which were preconditioned with 100 mg/kg 5-FU for 6 days. The infected cells were then coinjected into lethally irradiated recipient mice along with 2×10^5 CD45.1 competitor cells to ensure a competitive environment. The recipient mice were analyzed for the repopulation of CD45.2 donor cells at 3 to 16 weeks after transplantation. The number of hematologic cells in the peripheral blood (PB) was also evaluated 16 weeks after transplantation.

Flow cytometry

The frequency of LT-HSCs was evaluated by freshly isolating *Sirt3*-WT or *Sirt3*-KR BM cells and subjecting them to a flow cytometric analysis. Immunophenotypic Lin^- $Sca\text{-}1^+c\text{-}Kit^+CD135^-CD34^-$ LT-HSCs were evaluated or FACS-purified by staining with a biotinylated lineage cocktail (anti-CD3, anti-B220, anti-Mac-1, anti-Gr-1, and anti-Ter119 antibodies; BD Pharmingen), followed by incubation with streptavidin-PE/Cy5.5, anti-Sca-1-FITC, anti-c-Kit-APC, anti-Flk-2-eFluo450 (anti-CD135-eFluo450) and anti-CD34-PE antibodies (eBioscience). For the analysis of the repopulation ability of HSCs, the PB of recipient mice was collected, followed by the lysis of red blood cells and staining with anti-CD45.2-FITC, anti-CD45.1-PE, anti-CD3e-APC (for the T-lymphoid lineage), anti-B220-PE (for the B-lymphoid lineage), anti-Mac-1-APC, or anti-Gr-1-PE monoclonal antibodies (eBioscience; cells co-stained with anti-Mac-1 and anti-Gr-1 were deemed to be of the myeloid lineage). The cell cycle or apoptotic status was measured in purified LT-HSCs with Hoechst 33342/Pyronin Y or anti-Annexin V-PE/7-AAD (BD Pharmingen), followed by a flow cytometric analysis. Mitochondrial membrane potential and reactive oxygen species

(ROS) levels were assessed in purified LT-HSCs. For mitochondrial membrane potential measurement, cells were stained with 5 nM Tetramethylrhodamine (TMRM, Sigma) at 37 °C for 30 min. For ROS detection, cells were incubated with 5 μM 2',7'-dichlorodihydrofluorescein diacetate (H_2DCFDA, Invitrogen) at 37 °C for 30 min. After staining, cells were washed and resuspended in PBS, followed by flow cytometric analysis.

Cell culture

Immunophenotypic $Lin^-Sca\text{-}1^+c\text{-}Kit^+CD135^-CD34^-$ LT-HSCs or Lin^- cells were cultured with StemSpan serum-free medium (StemCell Technologies) supplemented with 10 ng/mL mouse SCF, 20 ng/mL mouse TPO, and 10 ng/mL FLT3-L (Peprotech) in a U-bottom 96-well plate. For the DHX58 or IRF7 overexpression experiments, the XZ201-*Dhx58*-HA-mCherry, XZ201-*Irf7*-HA-mCherry, or empty vector was cotransfected into 293T cells with the packaging plasmid pCL-ECO (2:1). The supernatant was collected at 48-72 h after transfection. Lin^- cells from *Sirt3*-WT or *Sirt3*-KR mice and 32D cells were infected with the retrovirus in the presence of 4 μg/mL polybrene, centrifuged at 800×g for 2 h, and then cultured for 48 h. RFP^+ 32D cells and RFP^+ Lin^- BM cells were sorted by FACS.

RNA-seq and quantitative RT-PCR

Sirt3-WT or *Sirt3*-KR $Lin^-Sca\text{-}1^+c\text{-}Kit^+CD135^-CD34^-$ LT-HSCs were sorted by flow cytometry, total RNA was extracted, and the samples were subjected to RNA sequencing at Shanghai Lie Bing Biomedical Technology Co., Ltd. A Gene Ontology enrichment analysis was performed with the Bioconductor package top GO. The analyses of enriched KEGG pathways were conducted using the Bioconductor package

GSEA. The candidate genes were further validated in *Sirt3*-WT or *Sirt3*-KR HSCs by quantitative RT-PCR. Briefly, first-strand cDNA was reverse transcribed using AMV reverse transcriptase (TaKaRa). RT-PCRs were performed according to the manufacturer's protocol with an Applied Biosystems 7900HT instrument. The mRNA levels were normalized to the level of β-actin RNA transcripts. The sequences of primers used are shown in Table S1.

β-galactosidase staining for senescence

The senescence of BM cells or 32D cells was performed with a senescence-associated β-galactosidase staining kit (Yeasen) according to the manufacturer's instructions. Briefly, the cells were fixed with fixative buffer for 15 min. After washes with PBS, the fixed cells were stained with fresh SA-β-Gal staining solution and incubated at 37 ℃ for 16 h. Images were acquired using an inverted fluorescence microscope (Nikon).

Immunofluorescence staining

For the immunofluorescence staining, *Sirt3*-WT or *Sirt3*-KR HSCs were sorted by flow cytometry and fixed with methyl alcohol at 4 °C for 15 min. The fixed cells were washed 3 times with PBS for 10 min each, permeabilized with a 0.1% Triton X-100 solution at room temperature for 15 min and blocked with 5% bovine serum albumin (Sigma) at room temperature for 1 h. The cells were then stained with γ-H2A.X (Abcam), p-TBK1 (Cell Signaling Technology), or STING (Cell Signaling Technology) antibodies at 4 °C overnight. The sections were then washed with PBS and incubated with the appropriate Alexa Fluor 488-conjugated secondary antibody (Thermo Fisher Scientific) or Alexa Fluor 555-conjugated secondary antibody (Thermo Fisher Scientific) at room temperature for 1 h. Nuclei were counterstained with DAPI (Thermo

Fisher Scientific) before imaging. Images were obtained with a Nikon A1 confocal microscope.

Luciferase reporter assay

The luciferase reporter vector pGL4.27 containing the promoter was constructed to identify the transcriptional regulation of *Gata2, Mllt3, Gata1* and *Pu.1* by IRF7. The indicated concentrations of the pLVX-*Irf7*-strepII-GFP (or negative control vector) were cotransfected with pGL4.27 promoter reporter vectors into 293T cells. Luciferase activities were measured using a luciferase reporter system (GloMax® Multi Instrument) 24 h after transfection. Relative luciferase activity was calculated as the ratio of firefly luciferase to Renilla luciferase activity.

Chromatin immunoprecipitation (ChIP) assays

ChIP assays were performed using a ChIP Assay Kit (Beyotime, P2078). 293T cells were cotransfected with pLVX-*Irf7*-strepII-GFP and pGL4.27-*Gata2*-promoter, pGL4.27-*Mllt3*-promoter, pGL4.27-*Gata1*-promoter or pGL4.27-*Pu.1*-promoter, crosslinked with 1% formaldehyde (Sigma) at 37 °C for 10 min, and then incubated with anti-IRF7 antibodies (Cell Signaling Technology) or rabbit control IgG (Cell Signaling Technology) at 4 °C overnight. For the sample input, 1% of the sonicated precleared DNA was purified at the same time as the precipitated immune complex. The ChIP samples were purified with a Gel and PCR Clean-up Kit (Nucleospin). The IRF7-binding sequence was amplified by semiquantitative PCR using primers specific for the *Gata2, Mllt3, Gata1* or *Pu.1* promoter region, as listed in Table S1.

Western blotting

Lysates of FACS-purified BM cells or cell lines were electrophoresed on 10% SDS polyacrylamide gels and transferred onto PVDF membranes (Millipore). The membranes were blocked with 5% nonfat milk and then incubated with an appropriate antibody, followed by an incubation with an HRP-conjugated secondary antibody. For the detection of acetylation, the protein was incubated with H3K27ac (Cell Signaling Technology), H3K9ac (Cell Signaling Technology), or H3 (Cell Signaling Technology) antibodies.

Cleavage under targets and tagmentation (CUT&Tag) analyses

The CUT&Tag assay was conducted using the NovoNGS CUT&Tag 3.0 High-Sensitivity Kit (Novoprotein). Briefly, isolated *Sirt3*-WT or *Sirt3*-KR $Lin^{-}Sca\text{-}1^{+}c\text{-}Kit^{+}CD135^{-}CD34^{-}$ LT-HSCs were enriched with ConA beads and resuspended in primary antibody buffer containing the H3K9ac antibody or H3K27ac antibody. The suspension was then incubated overnight at 4 °C. Next, secondary antibody buffer containing the anti-rabbit IgG antibody (Abcam) was added, and the mixture was incubated for 1 h. The beads were washed three times with antibody buffer and subsequently incubated with the Protein A/G-Tn5 transposome for 1 h. The beads were resuspended in tagmentation buffer (10 mM $MgCl_2$ in ChiTaq buffer) and incubated at 37 °C for 1 h. The incubation was terminated by the addition of 10% SDS and an incubation at 55 °C for 10 min. DNA fragments were extracted using Tagment DNA extraction beads, and the libraries were amplified using 5x AmpliMix. The DNA libraries were further purified using DNA clean beads in preparation for sequencing and PCR. The H3K9ac or H3K27ac-binding sequence was amplified by semiquantitative PCR using primers specific for the *Irf7* and *Dhx58* promoter regions, as listed in Table S1.

Table S1. List of primer

Genotyping primers	**Sequences**
Sirt3-F	GGGACCATTACAGAGTGAAGA
Sirt3-R	CATACAGAGCCACAGACATACC
q-PCR primers	**Sequences**
Mouse-*P16*-F	ACATCAAGACATCGTGCGATATT
Mouse-*P16*-R	CCAGCGGTACACAAAGACCA
Mouse-*P21*-F	CGAGAACGGTGGAACTTTGAC
Mouse-*P21*-R	CCAGGGCTCAGGTAGACCTT
Mouse-*Mx1*-F	CCTCCCACATCTGTAAATCACTG
Mouse-*Mx1*-R	CGGTTTCCTGTGCTTGTATCA
Mouse-*Irf7*-F	CCCCAGCCGGTGATCTTTC
Mouse-*Irf7*-R	CACAGTGACGGTCCTCGAAG
Mouse-*Oas3*-F	TCTGGGGTCGCTAAACATCAC
Mouse-*Oas3*-R	GATGACGAGTTCGACATCGGT
Mouse-*Dhx58*-F	GGAAGTGATCTTACCTGCTCTGG
Mouse-*Dhx58*-R	TTGCCTCTGTCTACCGTCTCT
Mouse-*Gbp5*-F	CAGACCTATTTGAACGCCAAAGA
Mouse-*Gbp5*-R	TGCCTTGATTCTATCAGCCTCT
Mouse-*Trim30a*-F	AGAGTTGACTGGGAGAACCAA
Mouse-*Trim30a*-R	TGCAGCATTTCTAAGGTTGAGAG
Mouse-*Oas1g*-F	ATGGAGCACGGACTCAGGA
Mouse-*Oas1g*-R	TCACACACGACATTGACGGC
Mouse-*Pik3ap1*-F	TGGTCCCGGATGCCTCTTT
Mouse-*Pik3ap1*-R	CACAAGTCATTTCCTGCCAGT

Mouse-*Tlr4*-F	GCCTTTCAGGGAATTAAGCTCC
Mouse-*Tlr4*-R	GATCAACCGATGGACGTGTAAA
Mouse-*Ifit44*-F	CCTGGTTCAGCAAACACGAGT
Mouse-*Ifit44*-R	TGGCCTTGATGGAATATGTCCT
Mouse-*Parp14*-F	CTGTATCAGCCACCGCTCAAA
Mouse-*Parp14*-R	CAACCAGTGCCGAACTCTCTT
Mouse-*Csf1*-F	GGCTTGGCTTGGGATGATTCT
Mouse-*Csf1*-R	GAGGGTCTGGCAGGTACTC
Mouse-*Ly9*-F	GCCTCAGATCATCGTGGAATC
Mouse-*Ly9*-R	TTGCAGGTATAGGGTAGGTCG
Mouse-*Il-1β*-F	GAAATGCCACCTTTTGACAGTG
Mouse-*Il-1β*-R	TGGATGCTCTCATCAGGACAG
Mouse-*Il-6*-F	CTGCAAGAGACTTCCATCCAG
Mouse-*Il-6*-R	AGTGGTATAGACAGGTCTGTTGG
Mouse-*Hoxb4*-F	CAGAGCGATTACCTACCCAGC
Mouse-*Hoxb4*-R	ATTGGGGTTTACCGTGCTCAC
Mouse-*Bmi1*-F	GCCCCTACCTCCCTACAGAC
Mouse-*Bmi1*-R	GTTGAACTCGTCTCCGATCC
Mouse-*Mllt3*-F	TGGTGAATGTGACAAGGCATATC
Mouse-*Mllt3*-R	TGTCCAGCGAGCAAAGATCAA
Mouse-*Gata2*-F	CGACGAGGTGGATGTCTTCT
Mouse-*Gata2*-R	GCTGTGCAACAAGTGTGGTC
Mouse-*Pu.1*-F	ATGTTACAGGCGTGCAAAATGG
Mouse-*Pu.1*-R	TGATCGCTATGGCTTTCTCCA
Mouse-*Gata1*-F	GATGGAATCCAGACGAGGAA

Mouse-*Gata1*-R	ACAGGCCCTGACAGTACCAC
Mouse-*Cebpa*-F	CAAGAACAGCAACGAGTACCG
Mouse-*Cebpa*-R	GTCACTGGTCAACTCCAGCAC
Mouse-*Ikaros*-F	CTCGGCCATTCGTACATGGAA
Mouse-*Ikaros*-R	GGATACCTCTGCACCGTAGC
Mouse-*Pax5*-F	TCCCAGATGTAGTCCGCCAAA
Mouse-*Pax5*-R	TCCTGTCTCATAATACCTGCCAA
Mouse-*Ebf1*-F	GTCACCACAAGCATGAATGG
Mouse-*Ebf1*-R	TCTGACAACTGGTGCGAAAG
Mouse-*E2a*-F	GGGTGCCAGCGAGATCAAG
Mouse-*E2a*-R	ATGAGCAGTTTGGTCTGCGG
Mouse-*Sox4*-F	GACCTGCTCGACCTGAACC
Mouse-*Sox4*-R	ACTCCAGCCAATCTCCCGA
Mouse-*Bcl11a*-F	GCTGTGCAACTATGCCTGTG
Mouse-*Bcl11a*-R	ACTCGATCACTGTGCCATTTTT
Mouse-*Sod1*-F	AACCAGTTGTGTTGTCAGGAC
Mouse-*Sod1*-R	CCACCATGTTTCTTAGAGTGAGG
Mouse-*Sod2*-F	CAGACCTGCCTTACGACTATGG
Mouse-*Sod2*-R	CTCGGTGGCGTTGAGATTGTT
Mouse-*Txn1*-F	CATGCCGACCTTCCAGTTTTA
Mouse-*Txn1*-R	TTTCCTTGTTAGCACCGGAGA
Mouse-*Prdx1*-F	AATGCAAAAATTGGGTATCCTGC
Mouse-*Prdx1*-R	CGTGGGACACACAAAAGTAAAGT
Mouse-*Prdx2*-F	GGTAACGCGCAAATCGGAAAG
Mouse-*Prdx2*-R	TCCAGTGGGTAGAAAAAGAGGT

Mouse-*Prdx3*-F	GTCTCGACGACTTTAAGGGAAAA
Mouse-*Prdx3*-R	ACTGAAACTGCAACTACTTCACA
Mouse-*Prdx4*-F	CTCAAACTGACTGACTATCGTGG
Mouse-*Prdx4*-R	CGATCCCCAAAAGCGATGATTTC
Mouse-*Prdx5*-F	GGCTGTTCTAAGACCCACCTG
Mouse-*Prdx5*-R	GGAGCCGAACCTTGCCTTC
Mouse-*Prdx6*-F	AAGCTGTCTATCCTCTACCCTG
Mouse-*Prdx6*-R	GTGGGAACTACCATCACGCT
Mouse-*Gpx1*-F	AGTCCACCGTGTATGCCTTCT
Mouse-*Gpx1*-R	GAGACGCGACATTCTCAATGA
Mouse-*Gpx2*-F	GCCTCAAGTATGTCCGACCTG
Mouse-*Gpx2*-R	GGAGAACGGGTCATCATAAGGG
Mouse-*Gpx3*-F	CCTTTTAAGCAGTATGCAGGCA
Mouse-*Gpx3*-R	CAAGCCAAATGGCCCAAGTT
Mouse-*Txnrd1*-F	CCCACTTGCCCCAACTGTT
Mouse-*Txnrd1*-R	GGGAGTGTCTTGGACGGGA
Mouse-*Txnrd2*-F	AAACCAGGACTTTGAATCTGGAG
Mouse-*Txnrd2*-R	GATGTGGGGAACAGAGGTAGC
Mouse-*Txnrd3*-F	GGCAACAGGGTGATGATCTTC
Mouse-*Txnrd3*-R	CTGGAAAGTTCGGTCACATCC
Mouse-*Txndc17*-F	AGGGCAAGACCATTTTCGC
Mouse-*Txndc17*-R	CCCTCTCGAATGACTGGCTC
Mouse-*Glrx1*-F	GCTCAGGAGTTTGTGAACTGC
Mouse-*Glrx1*-R	AGAAGACCTTGTTTGAAAGGCA
Mouse-*Glrx*2-F	ATCGTCGTTTTGGGGGAAGTC

Mouse-*Glrx*2-R	GGAACAGTAAGAGCAGGATGTTT
Mouse-*Glrx*3-F	CAGTGGTGGAAGTCGGCTC
Mouse-*Glrx*3-R	GCCATGACATCGTTCATCTGT
Mouse-*Nox1*F	GGTTGGGGCTGAACATTTTTC
Mouse-*Nox1*-R	TCGACACACAGGAATCAGGAT
Mouse-*Nox*2-F	TGTGGTTGGGGCTGAATGTC
Mouse-*Nox*2-R	CTGAGAAAGGAGAGCAGATTTCG
Mouse-*Gsr*-F	GACACCTCTTCCTTCGACTACC
Mouse-*Gsr*-R	CCCAGCTTGTGACTCTCCAC
Mouse-*Glut2*-F	TCAGAAGACAAGATCACCGGA
Mouse-*Glut2*-R	GCTGGTGTGACTGTAAGTGGG
Mouse-*Glut3*-F	ATGGGGACAACGAAGGTGAC
Mouse-*Glut3*-R	GTCTCAGGTGCATTGATGACTC
Mouse-*Glut4*-F	GTGACTGGAACACTGGTCCTA
Mouse-*Glut4*-R	CCAGCCACGTTGCATTGTAG
Mouse-*Hk1*-F	CGGAATGGGGAGCCTTTGG
Mouse-*Hk1*-R	GCCTTCCTTATCCGTTTCAATGG
Mouse-*Pfkl*-F	GGAGGCGAGAACATCAAGCC
Mouse-*Pfkl*-R	CGGCCTTCCCTCGTAGTGA
Mouse-*Pfkm*-F	TGTGGTCCGAGTTGGTATCTT
Mouse-*Pfkm*-R	GCACTTCCAATCACTGTGCC
Mouse-*Gapdh*-F	AGGTCGGTGTGAACGGATTTG
Mouse-*Gapdh*-R	TGTAGACCATGTAGTTGAGGTCA
Mouse-*Pkm2*-F	TGTGGTCCGAGTTGGTATCTT
Mouse-*Pkm2*-R	GCACTTCCAATCACTGTGCC

Mouse-*Ldha*-F	TGTCTCCAGCAAAGACTACTGT
Mouse-*Ldha*-R	GACTGTACTTGACAATGTTGGGA
Mouse-*Mdh1*-F	AGATTGCCTTCAAAGACCTGG
Mouse-*Mdh1*-R	GCAGTTCGTATTGGCTGGGT
Mouse-*Mdh2*-F	TTGGGCAACCCCTTTCACTC
Mouse-*Mdh2*-R	GCCTTTCACATTTGCTCTGGTC
Mouse-*Idh1*-F	ATGCAAGGAGATGAAATGACACG
Mouse-*Idh1*-R	GCATCACGATTCTCTATGCCTAA
Mouse-*Idh2*-F	GGAGAAGCCGGTAGTGGAGAT
Mouse-*Idh2*-R	GGTCTGGTCACGGTTTGGAA
Mouse-*Idh3a*-F	TGGGTGTCCAAGGTCTCTC
Mouse-*Idh3a*-R	CTCCCACTGAATAGGTGCTTTG
Mouse-*Idh3b*-F	TGGAGAGGTCTCGGAACATCT
Mouse-*Idh3b*-R	AGCCTTGAACACTTCCTTGAC
Mouse-*Idh3g*-F	GGTGCTGCAAAGGCAATGC
Mouse-*Idh3g*-R	TATGCCGCCCACCATACTTAG
Mouse-*Aco2*-F	ATCGAGCGGGGAAAGACATAC
Mouse-*Aco2*-R	TGATGGTACAGCCACCTTAGG
Mouse-*Atp5i*-F	GAGAAGGCACCGTCGATGG
Mouse-*Atp5i*-R	ACACTCTGAATAGCTGTAGGGAT
Mouse-*Atp5o*-F	TCTCGACAGGTTCGGAGCTT
Mouse-*Atp5o*-R	AGAGTACAGGGCGGTTGCATA
Mouse-*Cox6b1*-F	ACTACCTGGACTTCCACCG
Mouse-*Cox6b1*-R	ACCCATGACACGGGACAGA
Mouse-*Cox18*-F	GGCCGCCTATCAGCACTAC

Mouse-*Cox18*-R	TGAGATAAGTCTCCGCATGTTCT
Mouse-*Ndufb5*-F	CAAGAGACTGTTTGTCGTCAAGC
Mouse-*Ndufb5*-R	TGTTCACCAGTGTTATGCCAAT
Mouse-*G6pd*-F	CACAGTGGACGACATCCGAAA
Mouse-*G6pd*-R	AGCTACATAGGAATTACGGGCAA
Mouse-*Pgd*-F	TGAAGGGTCCTAAGGTGGTCC
Mouse-*Pgd*-R	CCGCCATAATTGAGGGTCCAG
Mouse-*Actin*-F	GGCTGTATTCCCCTCCATCG
Mouse-*Actin*-R	CCAGTTGGTAACAATGCCATGT

Luciferase primers	**Sequences**
Mouse-*Mllt3*-promoter-F	CCTGAGCTCGCTAGCCTCGAGGTGCAAACGC GGAATGGTCACC
Mouse-*Mllt3*-promoter-R	CAGTACCGGATTGCCAAGCTTCGAGCTAGCCA TGCCTGGGGG
Mouse-*Gata2*-promoter-F	CCTGAGCTCGCTAGCCTCGAGTCCCCCTCCCA CAGACATACAGAAA
Mouse-*Gata2*-promoter-R	CAGTACCGGATTGCCAAGCTTCGACTGCGGCG CGGTGGGC
Mouse-*Gata1*-promoter-F	CCTGAGCTCGCTAGCCTCGAGATAAAGCCTAA CTCTAACAGACCC
Mouse-*Gata1*-promoter-R	CAGTACCGGATTGCCAAGCTTCTTGGATATGG AGCTGGTAT
Mouse-*Pu.1*-promoter-F	CCTGAGCTCGCTAGCCTCGAGCTCTGATCAAA TGACTTGGCCCCA

Mouse-*Pu.1*-promoter-R	CAGTACCGGATTGCCAAGCTTAGGGGCGGTG AGGGAAAACC
Mllt3-F (for ChIP)	ACTCTTACAGACTTGGTTGGGAAAT
Mllt3-R (for ChIP)	TAACGGGAAGGAGGTTTCCTGGA
Gata2-F (for ChIP)	GACTATTAAAGATGGAAACAAATGCATG
Gata2-R (for ChIP)	GGGTTGAAGGTCACAGCACG
Gata1-F (for ChIP)	CCCCTCATGATGGCTCTTGGG
Gata1-R (for ChIP)	CCAAAGAGAAGGCAAAGACC
Pu.1-F (for ChIP)	CTCTGATCAAATGACTTGG
Pu.1-R (for ChIP)	AAAGACGTGGCCACCACAT
CUT&Tag primers	**Sequences**
Irf7-F (for q-PCR)	CTGAACCTAGGTGACCACAAGTTC
Irf7-R (for q-PCR)	CAGTCTGGGAGAATCAAAGTAGATG
Dhx58-F (for q-PCR)	CCCTACCAGTGGGAAGTGATCTTAC
Dhx58-R (for q-PCR)	AGCCATCTCCTGAACCAAGG